

Characterizing the impacts of seismic lines on the water budget of a Boreal Watershed in Alberta (Western Canada)

Daniels Kononovs^{a,b,c,*}, Christine Rivard^b, Dani Degenhardt^c, Katherine N. Snihur^a, Daniela Gutierrez-Rueda^a, Cody N. Lazowski^a, Kelly J. Rozanitis^a, Baptiste Coutret^a, Kurt O. Konhauser^a, Daniel S. Alessi^a

^a University of Alberta, Department of Earth and Atmospheric Sciences, Edmonton, AB, Canada

^b Geological Survey of Canada, Natural Resources Canada, Québec, QC, Canada

^c Canadian Forest Service, Natural Resources Canada, Edmonton, AB, Canada

ARTICLE INFO

Keywords:

Seismic lines
Hydrology
Canadian boreal forest
Alberta
1-D modeling
Critical zone monitoring

ABSTRACT

Study region: A 706 km² watershed located in a heavily industrialized region near Fox Creek, Alberta, Canada.

Study focus: Petroleum exploration has increasingly disturbed boreal ecosystems in North America. Seismic lines are one of the major footprints of the petroleum industry: they form cleared linear corridors in forests and their regeneration is generally poor. For this study, field measurements of soil, vegetation, water and snow were conducted on 5 paired (seismic line and adjacent undisturbed area) sites located in lowland and upland ecosites, and a 1-D physically based hydrologic model, the Simultaneous Heat and Water Model (SHAW), was used to investigate the impacts of seismic lines on the water budget over a year.

New hydrological insights for the region: Field measurements indicate that parameters, including soil water content and temperature, vary according to a complex combination of factors and are highly site-specific between seismic lines and undisturbed areas. Hydrological modeling of the two ecosites (lowland and upland) showed up to a 33 % reduction in evapotranspiration and a decrease in percolation (leading to none) below the root zone on seismic lines. Considering that there are 2300 km of seismic lines in the study area and that 36 % of the forest has been cleared for industrial activities, these results suggest that the water budget is impacted by anthropogenic lineaments. Climate change will likely intensify these impacts.

1. Introduction

The “Critical zone” (CZ) describes the heterogeneous, near-surface environment that extends from the top of the vegetation canopy to the underlying groundwater. This zone is responsible for controlling hydrologic processes such as runoff, infiltration, evapotranspiration (ET), and the transport and fate of metals, nutrients and contaminants (Brantley et al., 2007; Richardson, 2017). The CZ in Canadian boreal forests is particularly sensitive to anthropogenic climate forcing, leading to significant changes in the region’s carbon and hydrological cycles (Tam et al., 2019; Wang et al., 2021). With a predicted temperature increase of 4–11°C due to greenhouse gas (GHG) emissions by the end of the 21st century (Gauthier et al., 2015) and a predicted overall increase in ET (Wang

* Corresponding author at : University of Alberta, Department of Earth and Atmospheric Sciences, Edmonton, AB, Canada
E-mail address: kononovs@ualberta.ca (D. Kononovs).

et al., 2016, 2021), the boreal forests of western Canada could face more frequent and/or severe drought-like conditions in the near future (Wang et al., 2014; Tam et al., 2019) making it imperative to understand the hydrological cycle in this region in order to manage water resources sustainably. While much of the framework of critical zone science is built upon principal themes of soil science and hydrology/hydrogeology, their integration with other disciplines (such as vegetation, climate change and landscape changes) for broader theoretical understanding and quantitative modeling is pivotal for critical zone science (Richardson, 2017).

In addition to climate change, the CZ is further impacted by various anthropogenic disturbances which, over large areas, tend to accumulate and intersect over time and space (Wei and Zhang, 2010; Wei et al., 2022). A major disturbance in Canadian boreal forests are seismic lines created during the early stages of petroleum exploration (Dabros et al., 2018). Pasher et al. (2013) estimate that seismic lines comprise approximately 46 % of all linear features in Canadian boreal forests. Conventional seismic lines (between 5 and 10 m wide), constructed using bulldozers to produce a vegetation free landscape suitable for seismic surveys, were used up until the end of 20th century (Lee and Boutin, 2006; Braverman and Quinton, 2016). A study on early conventional seismic lines made during the summers in the 1960's showed that their construction resulted in the removal of roots and the top layer of soil, which may take several decades to regenerate (Bliss and Wein, 1972). Since the 1990s, low-impact 3D seismic lines have become more common than conventional seismic lines. These narrower lines (< 5 m) are created using a mulcher which is thought to have a smaller footprint and less disturbance over the long-term (Dabros et al., 2018).

There is no regulation in Canada that requires the restoration of seismic lines back to their original state, as it was initially assumed that these footprints would naturally regenerate over time (Dabros et al., 2018; Davidson et al., 2020). However, the recovery of seismic lines to their pre-disturbance state is influenced by a myriad of factors including: ecosite type, seismic line characteristics (width, length, aspect), disturbance history, landscape features, and subsequent line reuse (Van Rensen et al., 2015). It has been shown that the moisture content of landscapes affected by seismic lines is a major factor that controls the degree of woody vegetation recovery (Lee and Boutin, 2006; Van Rensen et al., 2015) with particular sensitivity in lowland ecosites. For example, a study in the Western Boreal Plains region of Alberta (Lee and Boutin, 2006) found that following a significant lag time (~35 years), upland ecosites are more likely to recover to > 50 % woody vegetation compared to lowland black spruce forests, which show minimal to no recovery.

This paper presents a study which aimed to investigate the impacts of seismic lines on soils and vegetation based on intensive fieldwork and monitoring, and their consequences on the various components of the water budget over the course of a year for a 706 km² watershed in a heavily industrialized region of west-central Alberta, Canada (Fig. 1). The climate in this region is one of long-term moisture deficit where precipitation (P) is less than, but close to, potential evapotranspiration (PET), typically at values of

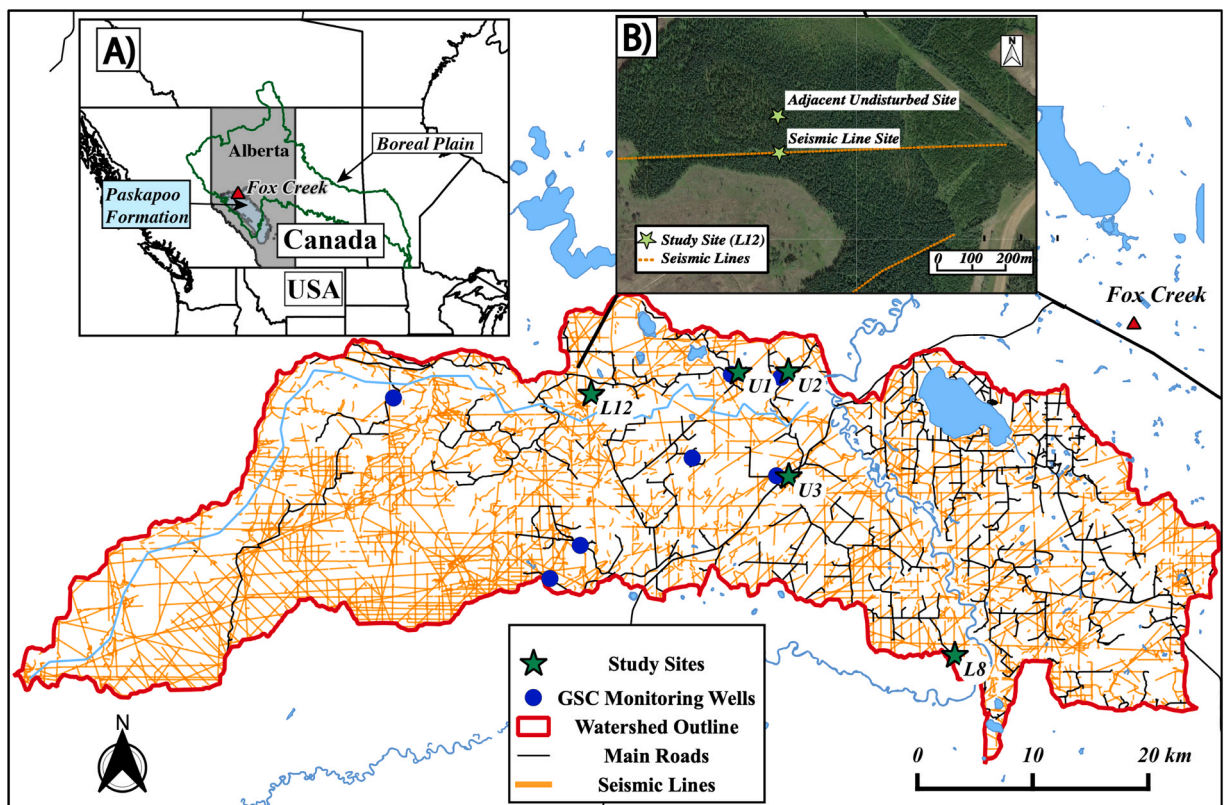


Fig. 1. Map of the watershed study area near the town of Fox Creek, Alberta (western Canada), showing the five field sites. Inset map A shows western Canada, with the province of Alberta in grey, the delineation of the Boreal Plains Ecozone in green, and the Paskapoo Formation in light blue. Inset map B shows the location of instrumentation installed at each paired site.

520 mm and 480 mm, respectively (Devito et al., 2012). Petroleum exploration and production has occurred in this region since the late 1950's (Fox Creek Historical Association, 1992). By end of 2022, approximately 1350 oil and gas (O&G) wells had been completed in the Duvernay Formation within the study area (AER, 2023). Intensive O&G exploration activities in the region have led to seismic lines accounting for 61.4 % of all linear disturbances in this watershed, making them ubiquitous throughout the study area (see Fig. 1). With a mean density of 3.4 km/km² but having a narrow width, they account for only approximately 2 % of the total watershed area (Le et al., 2023). They represent, however, only a fraction of the other infrastructure (roads, O&G well pads, pipelines) that has required forest clearance and for which the rationale, methodology and results of this study could also be applied. The loss of forest in the study area to various industrial activities since the 1950s has been estimated at around 36 % by Le et al. (2023).

To investigate the impact of disturbed areas, notably seismic lines, several sites were instrumented within the watershed as part of this study to collect and monitor soil and soil water data at different depths in the vadose zone, along with meteoric water sampling, to better understand the evolution of the physio-chemical properties along vertical soil profiles. In addition, soil-moisture and temperature were monitored as a function of depth. While the effects of seismic lines on vegetation regeneration (Bliss and Wein, 1972; Dabros et al., 2018, 2017; Lee and Boutin, 2006; Van Dongen et al., 2023; Van Rensen et al., 2015), soil characteristics (Davidson et al., 2020; Weiland et al., 2023), and forest fire potential have been investigated (Weiland et al., 2023), no study has yet focused on their effects on the various components of the water budget and integrated these data into a physically-based 1-D hydrological model to simulate their values over the course of a year.

This study integrates local field data from seismic lines and their adjacent undisturbed areas into a 1-D hydrologic model that accounts for snow, residue, soil, and plant canopy physics to estimate a time-distributed water budget to further our understanding of processes at play, in particular to investigate ET and percolation, which have been estimated using other methods. This study was part of a larger project on environmental cumulative effects of O&G activities in this region, which has been one of the most prolific oil and gas producing regions in Canada over the past 50 years (Rivard et al., 2023).

2. Study area & methods

2.1. Description of the study area

The study area is located in the province of Alberta, Canada's largest oil and gas producer, accounting for around 80 % of the country's total oil production (AGS, 2023). It resides in the Boreal Plains (BP) ecozone and corresponds to a 706 km² watershed near the Town of Fox Creek, in west-central Alberta, about 220 km northwest of the city of Edmonton (54.4009 ° N, 116.8045 ° W) (Fig. 1). The watershed is located to the east of the Rocky Mountains and is within the lower foothills natural subregion of Alberta. Most ecosites in this subregion have mesic moisture and medium nutrient regimes and the soils are moderately to well drained in mid-slope to level positions (Beckingham and Archibald, 1996). These ecosites are comprised of aspen and white spruce (*Picea glauca*) trees with an

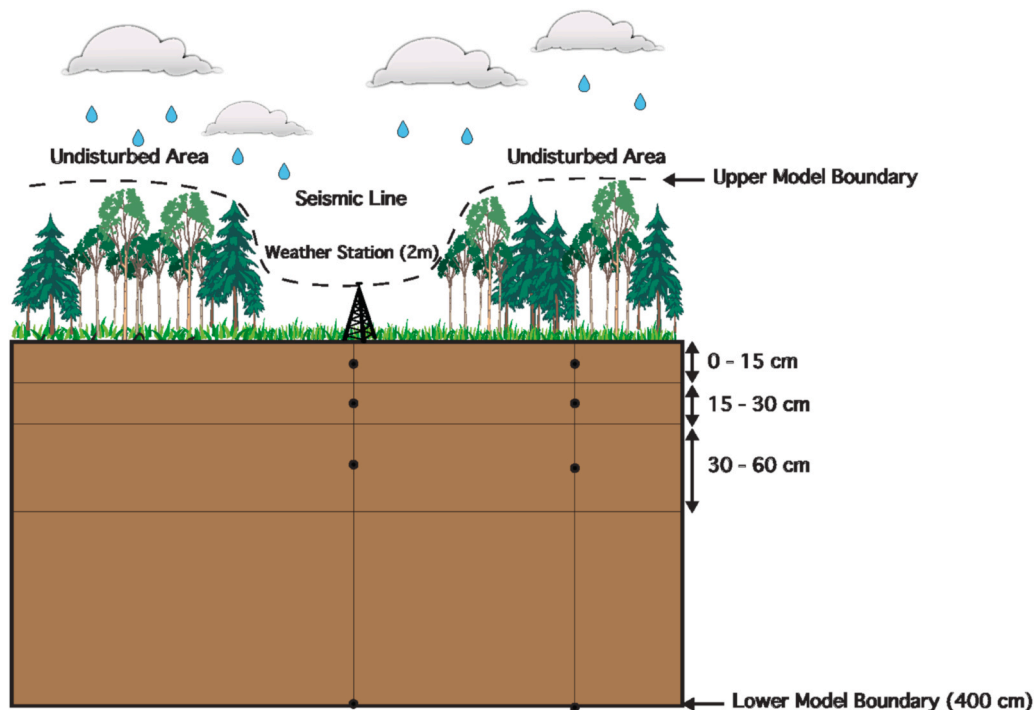


Fig. 2. Conceptual model used to develop the models with the SHAW model, showing soil layers and boundary conditions.

understory of low-bush cranberry (*Viburnum edule*), twin flower (*Linnaeus borealis*), and prickly rose (*Rosa acicularis*) shrubs and a high forb and grass diversity (Beckingham and Archibald, 1996). Boreal peatlands (bogs and fens) are also common in the study area and are characterized as regions with waterlogged soils and at least 40 cm of peat accumulation. Vegetation in bogs for the study region are characterized by black spruce (*Picea mariana*), Labrador tea (*Ledum groenlandicum*), and sphagnum mosses due to acidic groundwater that is poor in nutrients (Knapik and Lindsay, 1983).

The region is underlain by Upper Cretaceous – Paleocene bedrock, which is an assemblage of non-marine mudstones, siltstones, and sandstones (Atkinson and Hartman, 2017). The Paskapoo Formation is the main regional aquifer in the area (Fig. 1), consisting of a complex succession of mudstone and siltstone with interconnected sandstone channels that spans approximately 65 000 km² of the province (Lyster and Andriashek, 2012). The bedrock is overlain by thin (generally < 20 m in the study area) unconsolidated Paleogene-Quaternary surficial sediments, which are mainly comprised of glacial and fluvial deposits that are less permeable in the northern half of the Paskapoo Formation than in its southern extent (Atkinson and Hartman, 2017; Hughes et al., 2017).

Evapotranspiration (ET) in Alberta is estimated to comprise 74 % of the total annual precipitation (Islam, 2013). However, ET varies, and in the BP ecozone, it can be greater than precipitation (Devito et al., 2005). For the study area, the average annual evapotranspiration has been estimated to be nearly 90 % of the annual precipitation (495 mm/y versus 552 mm/y of total precipitation) (Guarin-Martinez, 2022), very close to the value found by Smerdon et al. (2019) for the town of Fox Creek (88 %). The coldest temperatures occur in January and the warmest temperatures occur in July, with monthly means of –11 and 15°C respectively, based on the Fox Creek Junction weather station record (1991–2011). The precipitation and evapotranspiration are highest in the summer.

2.2. Study sites selection, setup, and instrumentation

A paired site model was used for this study, including one location on a seismic line and another at least 20 m away from the edge of the first site, in the adjacent natural undisturbed area (an example is provided in Figs. 1 and 2). Overall, five study sites were selected: three upland sites (U1 to U3) and two lowland sites (L8 and L12) (Table 1). All seismic lines were oriented east-west. Equipment installed in June 2021 on all sites included: rainwater collectors, suction lysimeters, and soil moisture/temperature probes at varying depths (Table 1). Weather stations were installed at sites U1 and L8 in April 2022 to collect local meteorological data on both seismic lines and undisturbed areas, to estimate ET. Field photos showing selected sites and the instrumentation installed are available in the supplementary information (Appendix A, Figure A1).

2.3. Sample collection and analysis

2.3.1. Soil Solids

Soil samples were collected from each site at 15, 30, and 60 cm depths using a soil-core sampler of known volume (140 cm³). The organic rich soil horizon comprised of mainly decaying plant litter (i.e., the LFH layer) was removed prior to sampling. Samples were stored in Whirl Pak bags, sealed, and weighed prior to placing them in a drying oven. The samples were left to dry at 70°C for approximately 72 h for final dry weight for bulk density (BD) determination. For all samples, soil BD was determined for 0–15 and 15–30 cm depths.

Grain-size analysis was performed at Institut national de la recherche scientifique (INRS). Soil samples from site L12 could not be analyzed for grain-size as they were predominantly organic matter (peat) at all sampling depths. X-Ray diffraction (XRD) analysis was conducted at the University of Alberta EAS XRD Laboratory to identify the primary mineral phases present. Soil pH, EC, and water soluble ions were measured using the soil-to-water extraction method (Kalra and Maynard, 1991). Soil cation-exchange capacity (CEC) was determined using the ammonium chloride method (Kalra and Maynard, 1991). Total organic carbon (TOC), total inorganic carbon (TIC), dissolved organic carbon (DOC) and dissolved inorganic carbon (DIC) analyses were conducted at the NRAL laboratory at the University of Alberta using a Shimadzu TOC-L CPH Model Total Organic Carbon Analyzer. Soil organic matter (SOM) was calculated using soil organic content (SOC), based on the empirical relationship (Eq. (1)) derived by Waksman et al. (1930).

Table 1

General study site characteristics. Sites labelled with U and L indicate upland and lowland study sites, respectively. Line shot dates were obtained via SigMAP (2023), and numbers in parenthesis indicate the age of the line at the time of the beginning of this study (2021).

Study Site	Ecosite	Seismic Line		Equipment Installed					
				Suction Lysimeters			Soil Moisture Temperature Sensors	Weather Station	Rain Water Collector
Width (m)	Line Shot Date (age of line)	30 cm	60 cm	120 cm					
U1	low-bush cranberry (Aw)	8.3	1977 (45)	x	✓	✓	✓	✓	✓
U2	low-bush cranberry (Aw)	6.2	1977 (45)	✓	✓	✓	✓	x	✓
U3	low-bush cranberry (Aw)	6.2	1983 (40)	x	✓	✓	✓	x	✓
L8	bog (k)	6.2	1996 (27)	✓	✓	✓	✓	✓	✓
L12	bog (k)	6.9	1989 (34)	✓	✓	✓	✓	x	✓

$$\%SOM = 1.72 \times \%SOC \quad (1)$$

2.3.2. Weather data

Precipitation was measured year-round. Rain samples were measured from rain collectors (June 2021 – September 2022) and the weather stations (May 2022 – January 2023) whereas snow samples were collected from the ground. Snow depth and density were measured using a meter stick and a snow coring tube, respectively. The weather stations contained the following equipment: Hobo U30 Data logger, 5-W solar panel, Davis wind speed and direction sensor, temperature/relative humidity sensor, silicon pyranometer sensor (solar radiation), and a Davis rain sensor. The data logger was set to record data on an hourly basis. Field visits were conducted almost every month from June 2022 to January 2023.

Although there are many equations to calculate ET using weather data, the Penman-Monteith equation (Monteith, 1965; Allen et al., 1998) was chosen in this study as it is one of the most widely accepted and robust method for estimating ET. The Food and Agriculture Organization proposed in 1998 Eq. (2) (called “FAO 56”), which provides a reference evapotranspiration (ET_o).

$$ET_o = \frac{0.408\Delta(R_n - G) + \gamma \frac{900}{T+273} u_2(e_s - e_a)}{\Delta + \gamma(1 + 0.34u_2)} \quad (2)$$

where ET_o is the standardized reference evapotranspiration (mm day^{-1}), Δ is the slope of the vapor pressure curve ($\text{kPa } ^\circ\text{C}^{-1}$), R_n is the net radiation at the crop surface ($\text{MJ m}^{-2} \text{day}^{-1}$), G is the soil heat flux density ($\text{MJ m}^{-2} \text{day}^{-1}$), γ is the psychrometric constant that relates the partial pressure of water in air to the air temperature ($\text{kPa } ^\circ\text{C}^{-1}$), T is the mean daily air temperature at 2 m height ($^\circ\text{C}$), u_2 is the wind speed at 2 m height (m s^{-1}), e_s is the saturation vapor pressure (kPa), e_a is the actual vapor pressure (kPa), and $e_s - e_a$ is the saturation vapor pressure deficit (kPa).

ET_o calculations were made on a daily basis for the weather stations for the May 2022 – April 2023 period using the ET_o Calculator Software (FAO, 2012) and represents the evapotranspiration from a uniform grass crop 15 cm tall growing without water stress. This evapotranspiration estimate can be improved by calculating a crop specific evapotranspiration rate (ET_c) using Eq. (3) (Allen et al., 1998):

$$ET_c = ET_o * K_c \quad (3)$$

where ET_c is the crop evapotranspiration (mm day^{-1}) and K_c is the crop coefficient (a dimensionless empirical factor ranging between 0 and 1.4), which is generally used as an ecosystem evaporative stress index (Allen et al., 2011). The crop coefficient has been widely used as a parameter to estimate crop water demand by agricultural water managers (Allen et al., 1998, 2011). K_c values are influenced by many factors such as soil characteristics, climate, seasonality, vegetation cover and height, plant species distribution, and leaf area index (Allen et al., 1998). However, very few K_c values for the non-agricultural sector are available (although some K_c estimates have been found for various forest cover types, such as in Liu et al. (2017)) and these are known to be difficult to accurately estimate due to their heterogeneous nature and high soil water variability (Allen and Pereira, 2009; Allen et al., 2011). Since K_c is highly site-specific and no values have been found in the literature for the Canadian boreal forest, the ET_o values calculated using Eq. (2) from the weather stations were directly compared with those simulated by the Simultaneous Heat and Water (SHAW) model.

2.3.3. Soil water content and temperature

Data loggers (Meter Group, ZL6 data loggers) with soil moisture and temperature sensors (Meter Group, TEROS 10 and 5TM sensors) were installed at each site at 15, 30, and 60 cm depths to monitor soil water content (SWC) and soil temperature on an hourly basis. Data were recorded from June 2021 until October 2022.

2.3.4. Soil water and precipitation sampling

Suction lysimeters were installed using a handheld Dutch auger at depths of 30, 60 and 120 cm at each paired site to extract soil water for the analysis of soil solution chemistry. Upon each monthly site visit (from July to October 2021 and from May to October 2022, when the ground temperature was above 0°C), the suction lysimeters were evacuated of air using a vacuum pump by pressurizing to approximately 60 kPa and sealed allowing soil-water to accumulate in the suction lysimeters for approximately 4–24 h depending on the soil-moisture.

Monthly precipitation samples were collected from July 2021 to November 2022 to analyze $\delta^{18}\text{O}$ and $\delta^2\text{H}$ stable isotopes. During the winter months, fresh snowfall samples were collected and stored in Ziploc bags to minimize isotopic fractionation. Rainwater was collected in a simple rainwater collector, detailed in Gröning et al. (2012), designed to prevent evaporative fractionation, and a plastic container with a funnel on top and a drain on the bottom filled with approximately 1 cm paraffin oil to prevent evaporative losses.

Monthly soil and precipitation water samples were analyzed for $\delta^{18}\text{O}$ and $\delta^2\text{H}$ stable isotope ratios at the Froese Group Permafrost Lab at the University of Alberta using a Picarro L2130-i analyzer. Samples were passed through a $0.2 \mu\text{m}$ nylon membrane into 2.0 mL plastic vials ensuring no head space to prevent isotopic fractionation. The samples were plotted with the global meteoric water line (GMWL) (Eq. (4)) which describes the mean worldwide relationship between $\delta^2\text{H}$ and $\delta^{18}\text{O}$ isotope ratios for meteoric waters (Craig, 1961).

$$\delta^2\text{H} = 8 \delta^{18}\text{O} + 10\text{‰} \quad (4)$$

A local meteoric water line (LMWL) was established using the 2021 – 2022 precipitation data ($n = 39$ and $R^2 = 0.99$) using Eq. (5). The relative snow-water composition of groundwater was estimated using the same method outlined in Maule et al. (1994) and is detailed in the appendix (Appendix H).

$$\delta^2\text{H} (\text{‰}) = 7.44 \delta^{18}\text{O} (\text{‰}) - 6.80 \quad (5)$$

Soil and meteoric water samples were also titrated within 48 h of samplings using a Metrohm 905 Titrando at the University of Alberta (Edmonton, AB) to determine their alkalinity using a Gran Titration method. They were also analyzed for major cations and trace metals using an Agilent 8800 ICP-MS/MS at the University of Alberta Environmental Geochemistry Laboratory. Anions were quantified via a colourimetric method using a Thermo Gallery Plus Beermaster Autoanalyzer at the Natural Resources Analytical Laboratory (University of Alberta, Edmonton AB). The number of samples collected at the individual study sites for each analysis are summarized in Table B10 (see [supplementary information](#), Appendix G).

2.3.5. Vegetation

Percent cover vegetation, and tree height surveys were performed at each site on the seismic lines and their adjacent undisturbed areas (see [supplementary information](#), Appendix B, Table B1 and Figures B1 to B2). Monthly leaf area index (LAI) measurements were also obtained for the overstory (trees) and understory (grasses/shrubs) vegetative canopy from August – October 2022 at each site using a LAI-2200C Plant Canopy Analyzer (see [supplementary information](#), Appendix B, Table B2).

2.4. 1D Model SHAW

The simultaneous heat and water (SHAW) model is a soil vegetation atmosphere transfer (SVAT) model developed in 1989 (Flerchinger and Saxton, 1989) and has evolved into a vertical one-dimensional hydrologic model capable of simulating water, solute, and heat transfer within a system extending from the plant canopy to any specified soil-depth (Fig. 2). The model combines snow, residue, soil, and plant canopy physics into a single solution, while calculating interrelated water, heat, and solute fluxes in the system. Infiltration is modeled using the Green and Ampt (1911) method, whereas the Richards' equation is employed to describe the movement of water through the soil layers (Gosselin et al., 2016). The process of actual evaporation is directly incorporated into the energy budget equation, without relying on potential evaporation. Water and energy fluxes are interrelated and computed with Eq. (6) using site-specific meteorological data according to:

$$R_n + H + L_v E + G = 0 \quad (6)$$

where R_n is net radiation (W m^{-2}), H is sensible heat flux (W m^{-2}), $L_v E$ is latent heat flux (W m^{-2}), L_v is evaporation latent heat (J kg^{-1}), E is the total evapotranspiration of the multi-layer system ($\text{kg m}^{-2} \text{s}^{-1}$), and G is subsurface conductive heat flux (W m^{-2}) (Flerchinger, 2017a). The user specifies the number of plant canopy layers, soil-simulation depths and defines the lower boundary of the system with initial soil-temperature, water content, and textural properties (Flerchinger 2017a). The upper boundary of the system is defined with user-supplied meteorological data including precipitation, solar radiation, wind speed, air temperature and relative humidity.

The model built for this study contained three layers and reached a depth of 60 cm (Fig. 2). This very shallow model was developed because values for soil texture and SWC data series were only available for this interval, and field observations indicated that the root zone was in the vast majority of cases exceeded. Consequently, it was considered that most of the hydrologic processes in the critical zone could be simulated, and that values found at the base of the model could represent a proxy for recharge, enabling all the components of the water budget to be estimated. However, to more accurately simulate “deep” percolation (i.e., reaching the bottom of the model), the lower boundary condition was assumed to be a unit gradient from 60-cm downwards (i.e. assuming gravity flow). In this case, the SHAW model artificially extends the soil profile down to 4 m (the depth from which soil temperature is considered constant) where the soil temperature is estimated from the annual average air temperature (Flerchinger, 2017a). Previous work by Scanlon et al. (2002) recommends this approach for natural systems and studies using the SHAW model that do not have an independent measurement of “deep” percolation.

Simulations were carried out for four different cases: one for the undisturbed areas and one for the seismic lines for sites U1 and L8. Only these two sites, one representing upland and the other lowland ecosystems, were selected to be modelled due to limitations of available instrumentation, particularly the weather stations. The simulations were performed on a daily basis and results summarised to monthly values. The simulation period was from May 2022 to May 2023, during which site-specific weather data were collected.

Further details of the various numerical parameters and assumptions the SHAW model uses are described in the SHAW user's manual (Flerchinger, 2017a). The initial (and final) parameters used for soil and vegetation data are listed in Tables E1 to E3 of the [supplementary information](#) (Appendix F) along with their source.

The input parameters for vegetation (see [supplementary information](#), Appendix F, Table F1) are difficult to measure and are usually estimated using literature values (Flerchinger et al., 2012). Here, stomatal and plant resistance values were set according to the recommended values outlined in the user's manual (Flerchinger 2017b), while rooting depths were taken from the literature (Flinn and Wein, 1977; Strong and La Roi, 1983a,b). Typical albedo values for various vegetation types were derived from Betts and Ball (1997). Leaf water potential values were estimated via literature (Kaufmann, 1975; Caplan and Yeakley, 2010; Hébert and Thiffault, 2011). Transpiration threshold temperatures for plant species in the boreal forest are not well defined in literature and thus this value was left at the model default value of 7°C. The volumetric dry plant biomass estimates were within the range of typical boreal forest plant

communities (Proulx et al., 2015). LAI values were measured from August to October (see supplementary information, Appendix B, Table B2) and used as monthly inputs in the model. LAI values for June were assumed to be the same as September, and July the same as August. For the period from October to May, the LAI values were set to the minimum measurement recorded in October as this is the dormant season for vegetation.

Various soil textural parameters were measured in the laboratory (see supplementary information, Appendix C, Figure C1 and Table C1) and used as inputs for the model to calculate soil hydraulic properties to calibrate soil water content. Instead of using the default SHAW calculations, air entry potential and pore size index values were adjusted in the models using field observations to within 10 % of the model-calculated values to improve SWC calibration. Pore-size index was adjusted to within the model recommended values from 3.0 to 5.5.

Since the upper boundary of the model is limited by the height at which the weather data are collected, weather stations installed on seismic lines where the plant canopy is generally less than the height of the weather station (2 m) were assumed to provide appropriate inputs for the simulations. However, weather data collected from the adjacent undisturbed areas could not be used in the SHAW model, as the vegetation canopy is 10 – 20 m high in these areas. Thus, for the undisturbed areas, the weather data collected from the adjacent seismic line were used, assuming similar wind conditions among the seismic line and the top of the undisturbed forest plant canopy [pers. commun. with Dr. Flerchinger].

The simulations cover the May 2022 – April 2023 period, although the SWC dataset covers only part of it (data were monitored from September 2021–October 2022), as modeling had not initially been planned as part of this work and the SHAW model requires data from local weather stations, which were installed later in the project. The overlap interval (from May to October 2022) is, however, considered the most important, as less interactions between the soil and weather occur during the cold period (although snow melt can occur in May, depending on the year). Therefore, although not ideal, SWC data from November 2021 to May 2022 were used as a proxy for the model calibration (i.e., for comparisons between simulated and measured SWC data for the similar period the next year to fill the gap from November 2022 to May 2023).

To improve the SWC model simulations, manipulation of the saturated hydraulic conductivity (Ks) values for each soil layer was done within a reasonable limit, which was estimated from Ks values calculated using the Kozeny-Carman equation (see supplementary information, Appendix F, Table F4) for the soil samples from this study (from 0.04 cm/hr to 7.0 cm/hr), and Ks values estimated using Guelph permeameters in various areas within the upper 60 cm (not necessarily on sites U1 and L8) that ranged between 0.002 cm/hr to 5.1 cm/hr with a median of 0.37 cm/hr. Adjustment of the Ks values for each soil layer within this range did not show a significant impact on the simulated SWC due to the very shallow depths considered. Selecting Ks outside this range, (i.e., < 0.002 cm/hr) showed that it was possible to improve the SWC calibration, but this was deemed unrealistic based on data available (although some in situ tests using a Guelph permeameter carried out as part of the larger GSC project showed values of the order of 0.002 cm/hr).

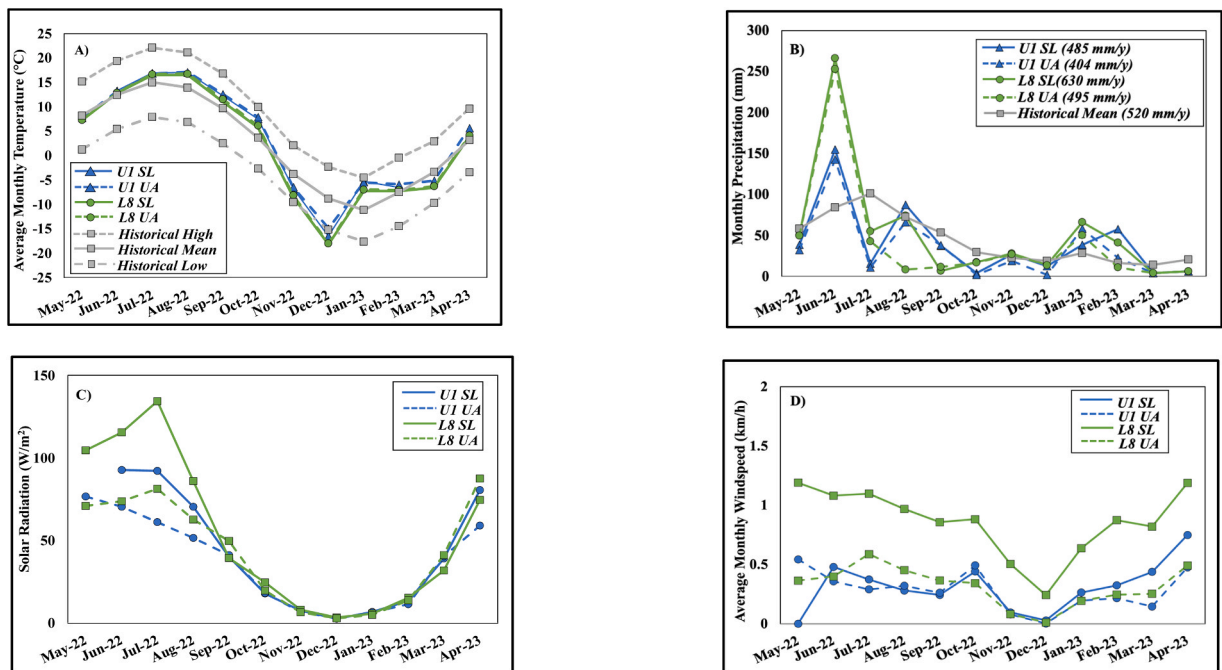


Fig. 3. Average monthly measured weather values for A) air temperature, B) total precipitation, C) net solar radiation, and D) wind speed among the study sites (U1 and L8, for on- and off-seismic line). Also depicted are the historical (21-years: 1991–2012) temperatures (low, mean, and high) and precipitation based on the Fox Creek Junction weather station. SL and UA denote seismic line and undisturbed area, respectively.

3. Results

3.1. Weather data

The average monthly measured annual air temperature, precipitation, windspeed, and net solar radiation for study sites U1 and L8 from May 2022 to April 2023 are shown in Fig. 3. Air temperature was similar among all four locations (Fig. 3A). Among the four sites, the recorded monthly high occurred in August and was 17.1°C, which was near the historical mean of the Fox Creek weather station, whereas the lowest monthly temperature occurred in December at -18.2°C, one month earlier than the historical mean, well below the historical low of -15.2°C. The seismic line on site U1 received a total of 485 mm of precipitation over this 12-month period, which is

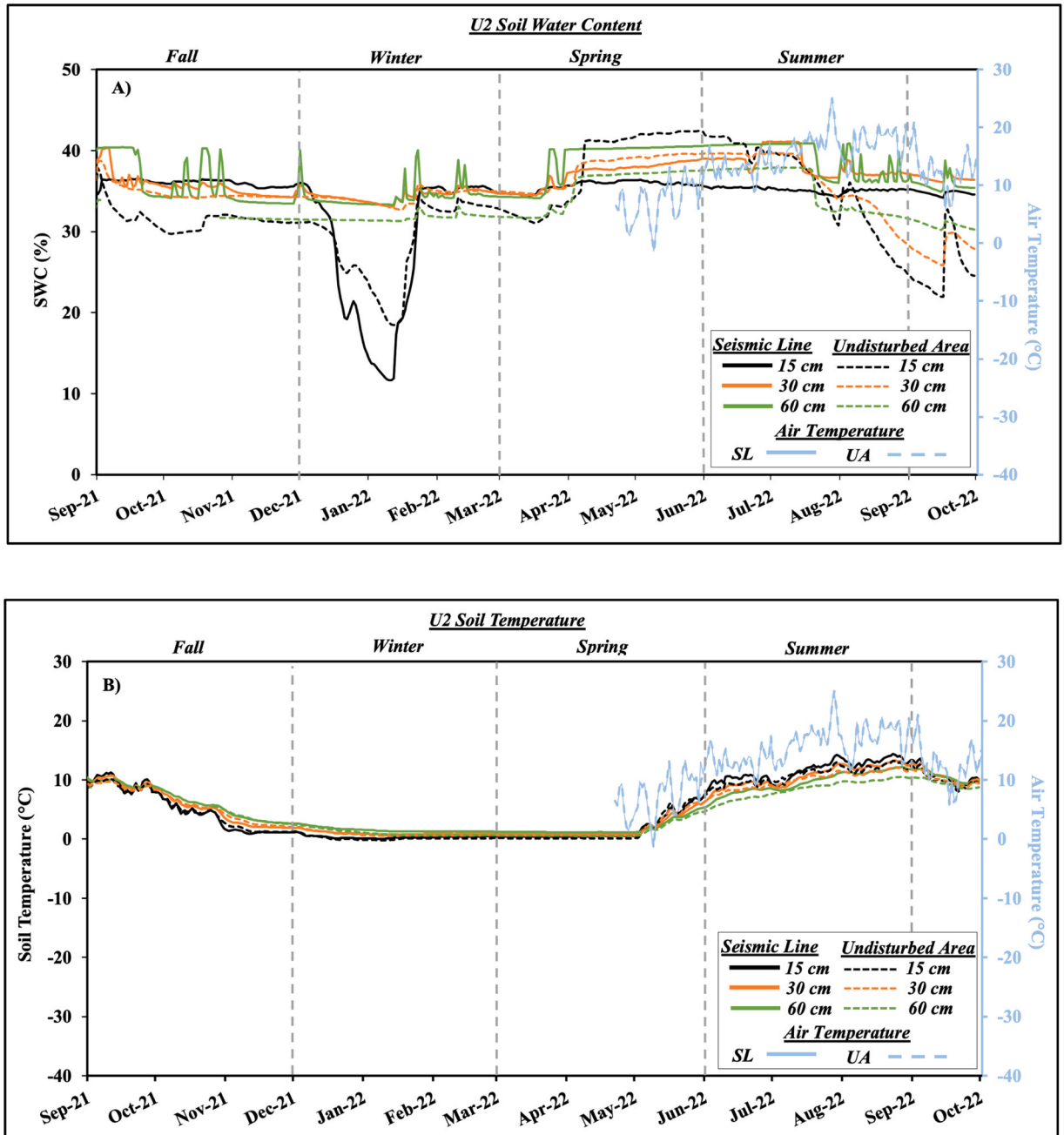


Fig. 4. A) Soil water content (SWC) and B) soil temperature plots for upland site 2 (U2) from September 2021 to September 2022. SL and UA denote seismic line and undisturbed area, respectively. Some data are missing in winter due to several consecutive days of low temperatures, which rapidly discharged the battery.

close to the historical mean of 520 mm, whereas the adjacent undisturbed area only received 404 mm (Fig. 3B). The seismic line on site L8 received 630 mm, which is 110 mm higher than the historical mean annual precipitation, whereas the adjacent undisturbed area received 495 mm.

Net solar radiation from May to August 2022 was higher on both seismic lines compared to the adjacent undisturbed areas, mainly due to the smaller and sparser vegetation. The largest recorded net radiation values occur in July when they reach up to 134 W/m². The largest difference in net radiation between the seismic line and undisturbed area also occurs in July, 31 W/m² and 53 W/m² for U1 and L8, respectively. Net radiation is lowest during the winter months and reaches its lowest value (approximately 3.0 W/m²) in December.

The average monthly windspeed variations were generally slightly greater on the seismic line at site U1 compared to the

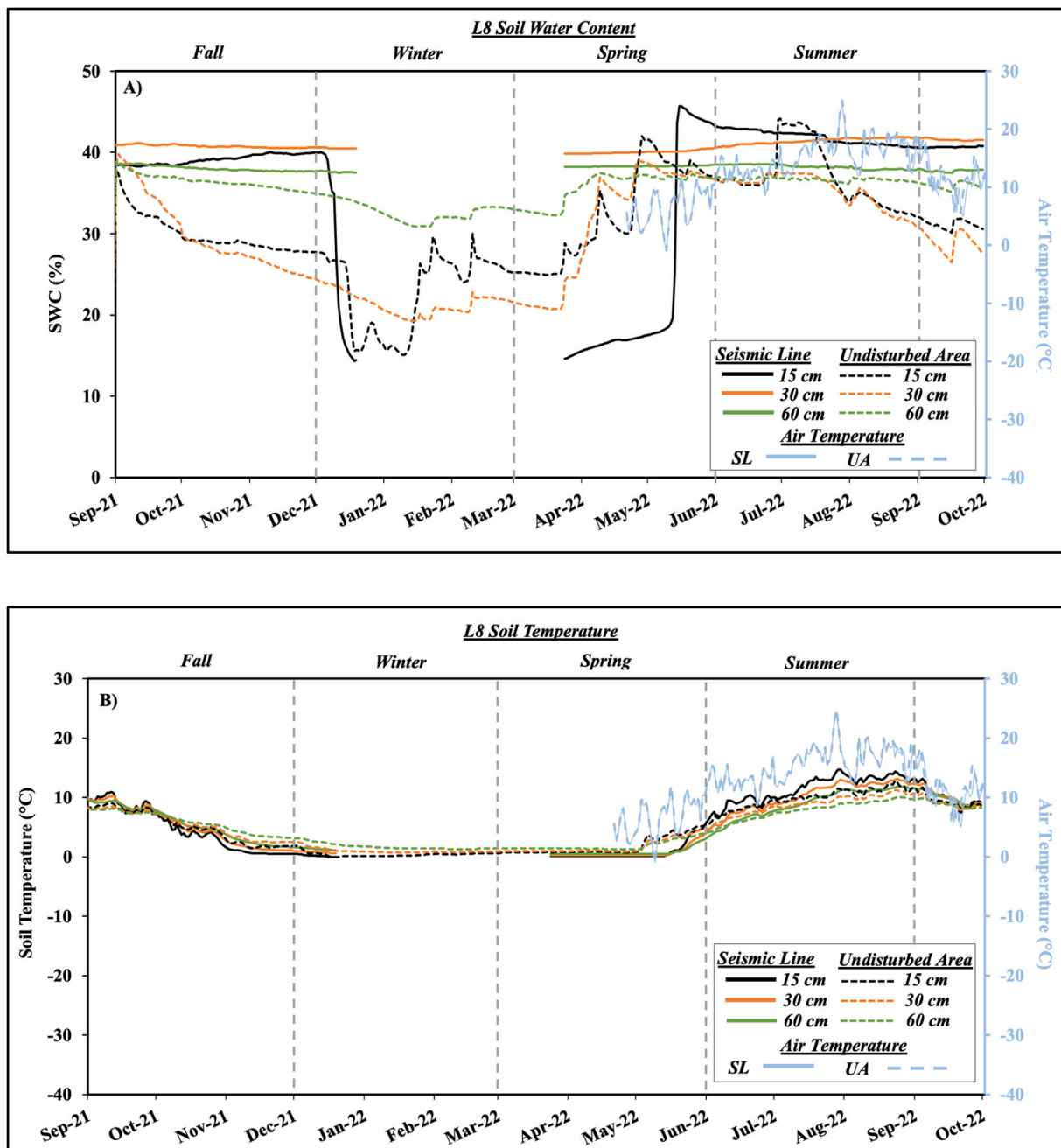


Fig. 5. A) Soil water content (SWC) and B) soil temperature plots for lowland site 8 (L8) from September 2021 to September 2022. SL and UA denote seismic line and undisturbed area, respectively. Some data are missing in winter due to several consecutive days of low temperatures, which rapidly discharged the battery.

undisturbed area, but not significantly (p -value of 0.05) greater. In contrast, the measured windspeed on the seismic line of L8 was significantly higher ($p < 0.001$), on an average by 2.7 times, compared to the adjacent undisturbed area (Fig. 3D).

3.2. Soil textural properties

Soil-samples from all study sites and depths were classified as silt-loam, except for the undisturbed area at site L8, which was a sandy loam (see [supplementary information](#), Appendix C, Figure C1). Soil BD values for 0–15 and 15–30 cm depths ranged from a low of 0.11 g/cm³ (L12 peat) to a high of 1.69 g/cm³ (U3 mineral soil) with a median of 1.04 g/cm³ (see [supplementary information](#), Appendix C, Table B1). These BD values are within the typical range for mineral soils of 1.0–1.8 g/cm³ (Brown et al., 2021).

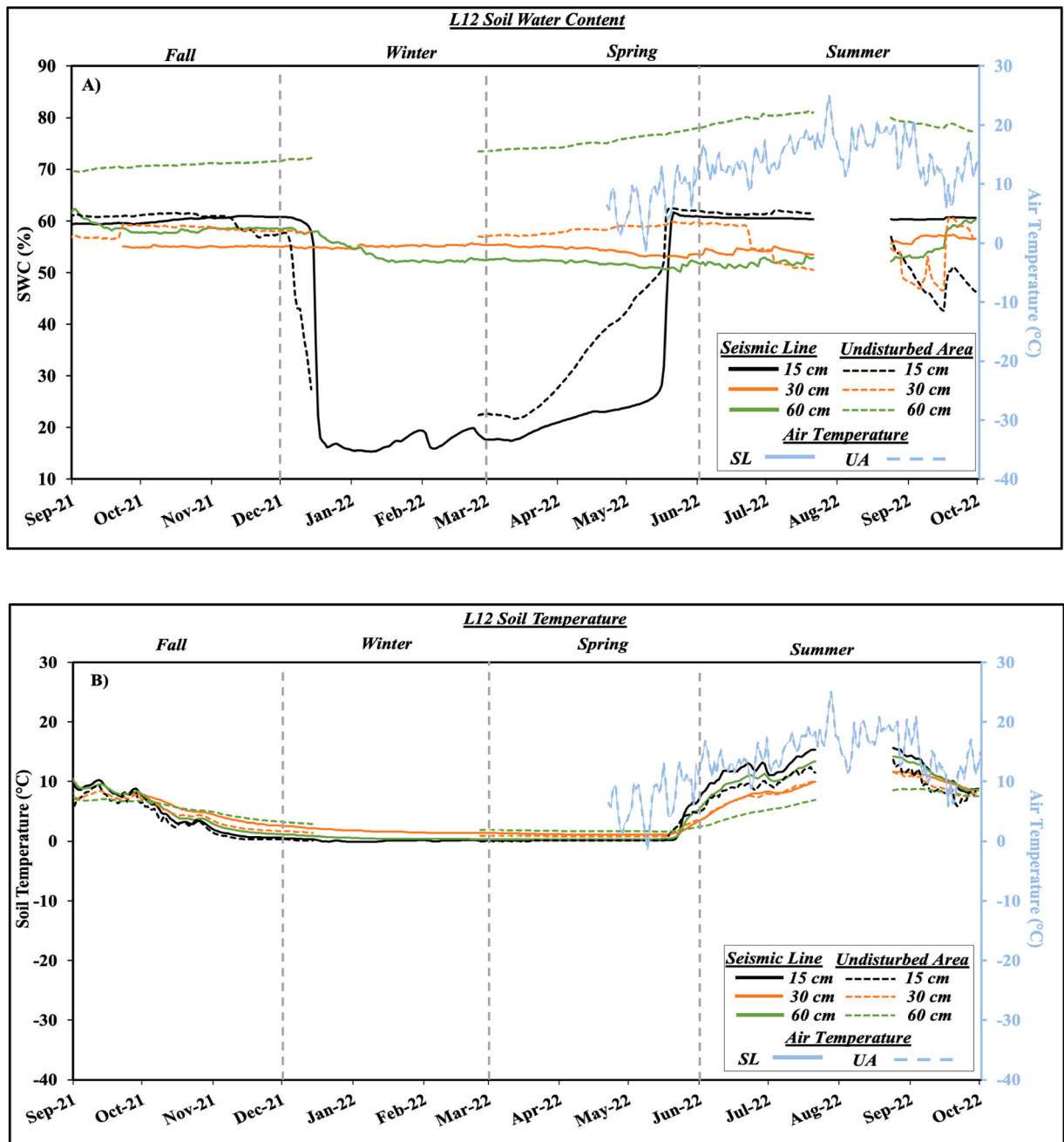


Fig. 6. A) Soil water content (SWC) and B) soil temperature plots for lowland site 12 (L12) from September 2021 to September 2022. SL and UA denote seismic line and undisturbed area, respectively. Some data are missing in winter due to several consecutive days of low temperatures, which rapidly discharged the battery.

Nonetheless, the BD measurements, especially in the upper 15 cm of the soil-profile, were up to 65 % higher on the seismic lines compared to the undisturbed sites (see [supplementary information](#), Appendix C, Table C1).

SOM content for the upland sites at 15 cm depth was greater in undisturbed areas than on seismic lines (see [supplementary information](#), Appendix C, Table C1). For instance, SOM content for sites U1, U2, and U3 was greater by factors of 6.9, 2.8, and 12.3, respectively, compared to the adjacent seismic line. However, for lowland sites L8 and L12, SOM content at 15 cm depth from the seismic line was greater by factors of 11.6 and 1.6 respectively. The relationship between site type and SOM content at 30 cm is less clear for upland and lowland sites.

3.3. Soil water content & temperature plots

Soil water content (SWC) and soil temperature data series are presented in [Figs. 4, 5 and 6](#) for sites U2, L8 and L12, respectively. Since the upland sites (U1, U2, and U3) all showed similar results, only U2 is presented. Data from U1 and U3 are available in the [supplementary information](#) section (Appendix E, Figures E1 and E2). The specific behavior of the two sets of data for sites U2, L8, and L12 are described in the [supplementary information](#) section (Appendix D).

The SWC for all study sites mainly ranged between 20 % and 40 %, except site L12, where the SWC reached up to 80 % due to its topographically low location and the accumulation of > 1 m thick peat. Temporal fluctuations in SWC were most evident in the shallow (15 cm) measurements and decreased with depth. The seismic line at site L8 generally had a higher SWC at all depths compared to the undisturbed area ([Fig. 5A](#)). This is likely due to the large soil textural contrast: a silt loam on the seismic line compared to a sandy loam in the undisturbed area.

In the winter, for all sites, soil frost development caused a significant drop in measured SWC at the shallow 15 cm depth but not for the 30 and 60 cm depths. Since this notable drop occurred at a depth of 15 cm, but not 30 and 60 cm, it suggests that a complete soil frost penetration is confined to the range between 15 and 30 cm. Some pore water can likely remain unfrozen below 30 cm, even when the soil temperature drops below 0°C. In fact, a soil temperature well below zero is often required to freeze pore water in smaller pores ([Ren and Vanapalli, 2019](#)). Following spring melt, SWC on the upland sites was higher on the undisturbed areas because of the higher SOM content (see [supplementary information](#), Appendix C, Table C1). During the summer, the undisturbed areas in the upland sites and lowland site L8 showed a larger decline in SWC compared to their respective seismic lines, likely due to enhanced plant water use. This was not true for the lowland site L12, which remained nearly saturated all year.

As expected, soil temperature generally follows air temperature patterns, but differences in temperature become less pronounced with increasing depth. During the winter, soil temperature increased with depth by about 1–2°C between 15 and 60 cm while the opposite trend ranging from 2 to 4°C occurs in the summer. Summer soil temperatures were always higher on the seismic lines, mainly due to their reduced canopy cover which enhances the amount of solar radiation reaching the soil surface and thus increasing its temperature more than the adjacent undisturbed area. Spring soil temperatures indicated that soil thaw initially occurred on the undisturbed areas. This is because of the delayed snow melt on seismic lines ([Haag and Bliss, 1974](#)), which have a higher albedo relative to undisturbed areas ([Dabros et al., 2018](#)). In the spring and fall, soil temperature trends varied among the seismic lines and undisturbed areas for the three sites.

3.4. SHAW model water budget

3.4.1. Calibration

The SHAW model has been used to simulate energy and water balances without calibration in many studies ([Flerchinger and Pierson, 1991](#); [Link et al., 2004](#); [Kang et al., 2005](#); [McNamara et al., 2005](#)). However, the representativeness of simulation results is improved when the model can be calibrated with field observations and can lead to more accurate estimation of crucial parameters for

Table 2

Model performance values for net radiation and soil water content (SWC) calibration. SL: seismic line, UA: undisturbed area, ME: model efficiency, RMSD: root mean square deviation, and PBIAS: percentage bias for each site.

Site	Net Radiation			SWC			
	ME	PBIAS (%)	RMSD (W/m ²)	Simulation Depth (cm)	ME	PBIAS (%)	RMSD (% SWC)
U1 SL	0.95	−14.5	0.4	15	0.6	5.4	4.4
				30	0.5	2.3	3
				60	0.8	−6.6	3.6
U1 UA	0.95	12.7	0.4	15	0.6	6.6	8.9
				30	0.3	−8.7	3.6
				60	0.5	−2.5	2.2
L8 SL	0.9	−20.7	1.0	15	−0.2	−2.9	24.4
				30	−99.8	−14.4	17.7
				60	−0.3	1	0.1
L8 UA	0.9	−10.2	1.0	15	0.7	−3.2	3.6
				30	0.7	−0.7	3.4
				60	0.01	−10.5	5.4

a given region (Flerchinger and Hardegee, 2004; Huang and Gallichand, 2006; Yin et al., 2010a, b), such as evapotranspiration in this case. In this study, the SHAW model was calibrated using net-solar radiation and SWC by comparing measured values with simulated ones and attempting to minimize the root mean square deviation (RMSD, also called root mean square error, RMSE). The results for the calibration are summarized in Table 2 and the figure showing these data series are presented in the supplementary information section, Appendix F (Figure F1).

To assess model performance, the model efficiency (ME, also called the Nash-Sutcliffe efficiency (i.e., NSE)), a widely used statistic for assessing the goodness of fit of hydrologic models, RMSD, one of the most commonly used measures for evaluating the quality of predictions, and percentage bias error (PBIAS), a measure of the average tendency of the simulated values to be larger or smaller than the corresponding observed ones, were calculated according to Eqs. (7) to (9) (Nash and Sutcliffe, 1970; Green and Stephenson, 1986).

$$ME = 1 - \frac{\sum_{i=1}^N (X_i - \hat{X}_i)^2}{\sum_{i=1}^N (X_i - \bar{X}_i)^2} \quad (7)$$

$$RMSD = \left[\frac{1}{N} \sum_{i=1}^N (X_i - \hat{X}_i)^2 \right]^{0.5} \quad (8)$$

$$PBIAS = \frac{1}{N} \sum_{i=1}^N (\hat{X}_i - X_i) \quad (9)$$

N is the total number of observations, X_i is the observed value at a given time step, \hat{X}_i is the simulated value at a given time step, and \bar{X}_i is the mean of the observed values (Yin et al. 2010a). ME describes the variation in measured values explained by the model with ME values from 0.0 to 1.0 being acceptable (1.0 is a perfect match between the model and observed data), while $ME < 0.0$ occurs when the observed mean is a better predictor than the model and, therefore, is considered an unacceptable performance (Yin et al., 2010). Lower values of RMSD indicate a better model performance. Lastly, PBIAS shows the percent deviation from model simulated values to the actual measured values. Negative values indicate a model bias of underestimation relative to the measured value, whereas positive values indicate a model bias to over-estimate the measured value. The ideal value for PBIAS is 1.0.

The SHAW model simulated net radiation trends very well (Table 2), as ME was > 0.9 across all sites and RMSD values ranged from 0.4 W/m^2 to 1.0 W/m^2 per day (see supplementary information, Appendix F, Figure F1). Nonetheless, the model consistently underestimated net radiation at both sites (U1 and L8), but by less than 20 % (between -12.7% and -20.7%) as indicated by the PBIAS value and shown in the graph of pairs of simulated and measured values at a given time (Fig. 7). The consistent underestimation of net radiation by the SHAW model at both sites can be attributed to various factors, including limitations in input data quality, parameter calibration, and representation of surface characteristics. Calibration of surface parameters, such as albedo and vegetation cover, is

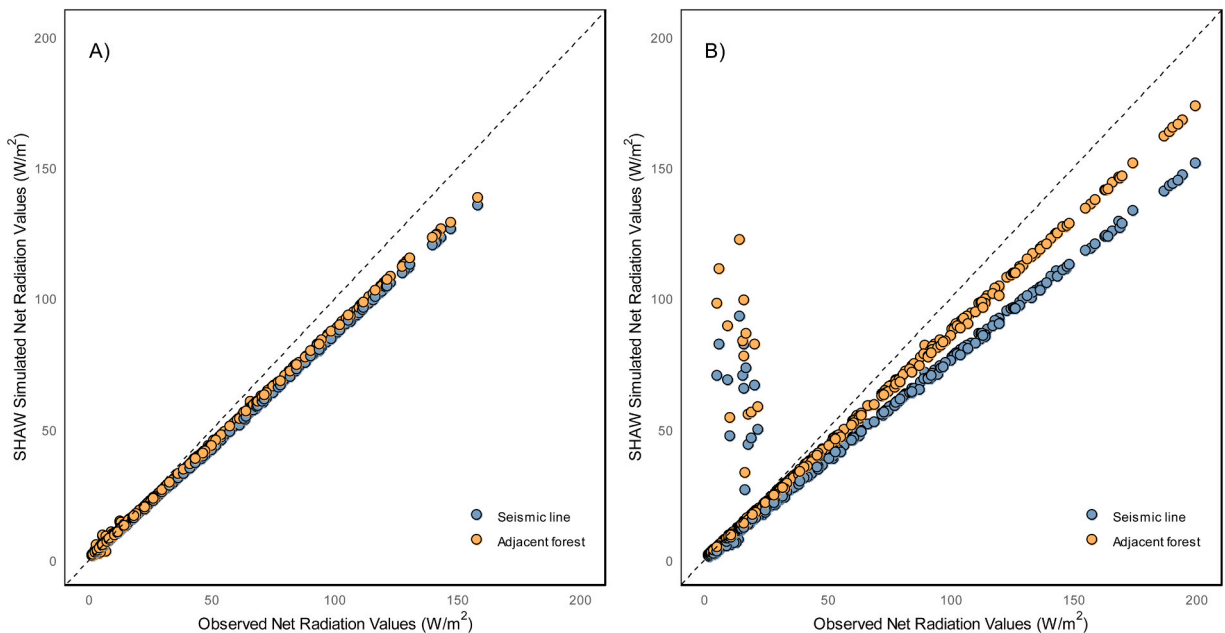


Fig. 7. Pairs of simulated versus observed values for net radiation values at a given time for A) site U1 and B) site L8. The dashed black line represents a line with a slope of 1.

crucial; if these parameters are not carefully fine-tuned, particularly albedo which affects reflection, the model may systematically under- or over-estimate net radiation. In this case, the model's simplified representation of vegetation and surface conditions (i.e. homogenous, representing only the dominant feature), while our sites featured complex canopies and variable soil properties, likely limited its ability to accurately simulate absorbed radiation, contributing to the underestimation of net radiation. Sensitivity analysis revealed that manipulating LAI, plant and soil albedo values and/or the extent of plant and residue cover did improve the PBIAS values to some extent. However, achieving a significant improvement would require values to be set beyond reasonable limits based on available data and our regional knowledge. This option was therefore discarded.

For site L8 (Fig. 7B), the simulated values for the seismic line are further away from the observed values, which can probably be attributed to a combination of factors, including the location of the weather station on the seismic line, the seismic line width and the vegetation characteristics, which can have an impact on the measured values, as well as some characteristics that could not be properly taken into account in the SHAW model, such as short vegetation with lower dry biomass (see [supplementary information](#), Appendix F, Table F1). Also, at site L8, the outliers located at observed values of about 20 W/m² appear to be due to the fact that the SHAW model predicted complete snowmelt in mid-February based on weather data (positive temperatures over several days). However, field verification confirmed that the snow cover had not completely melted.

Generally, the SHAW model yielded acceptable results for SWC simulations (Fig. 8; additionally, see [supplementary information](#), Appendix F, Figure F2). It is noteworthy that, as indicated in [Section 2.4](#), the cold period (from November 2022 to May 2023) for these data had to be taken from the previous year. For this reason, only an “acceptable” match was sought, to ensure that modeled and measured SWC data were within the same range. Most of the data series appear to be well distributed on either side of the 1:1 line, indicating that the model is capable of representing conditions satisfactorily (Fig. 8). Although only half of the ME values for the simulated SWC for site U1 are ≥ 0.6 (all being > 0), the RMSD is $< 10\%$ indicating a relatively good correspondence for site U1. For the seismic line on site L8, for which variations in SWC over time are very small (nearly constant values, see Fig. 5), ME is not good (< 0) but RMSD remains below 25%. The relatively linear sections of these data sets were mainly due to freezing conditions during the winter or to differences in soil conditions between the seismic line (rather silty/clayey) and the adjacent undisturbed area (rather sandy, see [supplementary information](#), Appendix C, Figure C1). For the undisturbed area of site L8, ME is very good (≥ 0.7) for two of the three depths, while the RMSD is small ($< 5.4\%$). As expected, most of the discrepancies are due to winter season data. The latter are described in detail in [Konoynovs \(2023\)](#), but because the SWC data for winter do not correspond to the simulated year, they are not discussed here. In most cases for the two sites, PBIAS remained below 10%, which is again considered acceptable.

3.4.2. Water budget components

The simulated results of the various water budget components for sites U1 and L8 are summarized in [Table 3](#). The dryness index ratios (ET:P) for the undisturbed areas at site U1 and L8 were 0.9 and 0.8, respectively, which are similar or close to the value estimated for this study area (0.9) by [Guarin-Martinez \(2022\)](#). These ratios are also in relatively good agreement with the province-wide work of [Devito et al. \(2005\)](#), who estimated average ET values around 0.9 (or 90% of total precipitation).

Comparatively, the dryness index ratios (ET:P) for the seismic lines of U1 and L8 were 0.8 and 0.6, respectively, indicating a wetter environment than their respective undisturbed areas. This is because of the decreased vegetation abundance on seismic lines (see [Figures A1 and A2](#)), which resulted in lower ET rates when compared to undisturbed areas. In particular, site L8 was very wet as it received approximately 138 mm more precipitation compared to site U1 over the growing season. Overall, ET was higher in undisturbed areas compared to the seismic lines by 34 mm and 117 mm for sites U1 and L8, respectively ([Fig. 9](#)). Compared to site L8, the smaller difference in ET among the seismic line and undisturbed area at site U1 is likely attributed to biomass values used for the

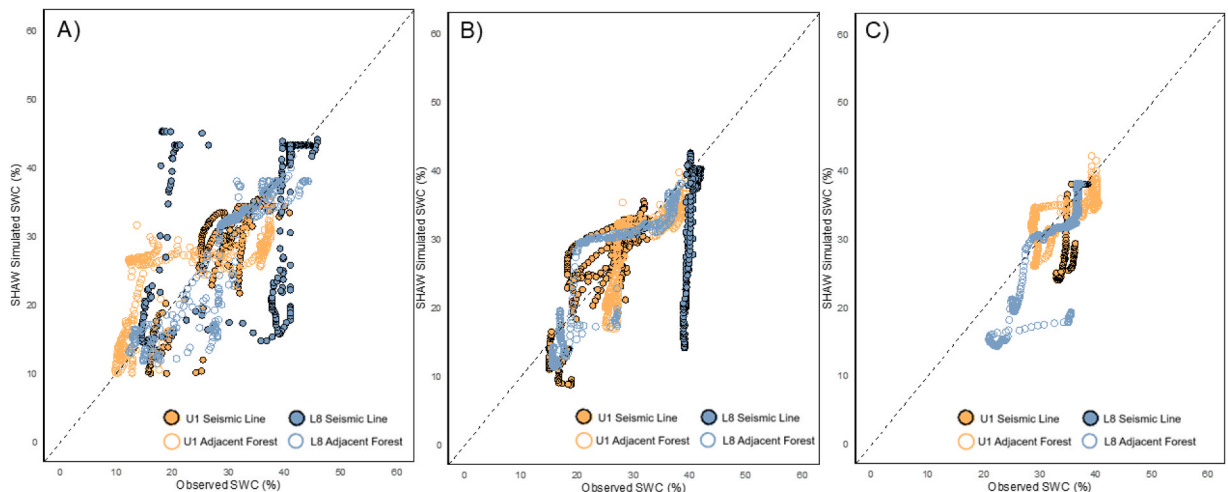


Fig. 8. : Pairs of simulated versus observed values for soil water content (SWC) at a given time for sites U1 and L8, for both disturbed (seismic line) and undisturbed (adjacent forest) areas at A) 15 cm, B) 30 cm and C) 60 cm depths. The dashed black line represents a line with a slope of 1.

Table 3

Simulated annual values (May 1, 2022, to April 30, 2023) for the various components of the water budget for all study sites. SL and UA denote seismic line and undisturbed area, respectively.

Site	Precipitation	Runoff	ET	Deep Percolation*	Change in Storage **	Cumulative Simulation Error (mm)* **
U1 SL	472.4	57.6	380.4	0.0	21.8	-6.9 (-1.5 %)
U1 UA	472.4	3.8	414.4	47.8	-12.9	-0.7 (-0.2 %)
L8 SL	610.2	240.7	355.3	0.0	-8.6	-14.9 (-2.4 %)
L8 UA	610.2	247.6	472.11	21.5	-127.0	-7.8 (-1.3 %)

* “Deep” percolation corresponds to the water flux beyond the deepest soil node (400 cm in this study).

** The change in storage term is comprised of soil storage (negative values indicate water was used up, whereas positive values indicate water was gained).

***A negative simulation error value indicates an underestimation of the cumulative water balance by the model. In parenthesis is the percentage error determined from the cumulative simulation error divided by the total precipitation the area receive.

seismic line vegetation (see Table E1), which were relatively similar among the line and undisturbed area for site U1 compared to the much larger difference for site L8.

The average simulated ET rates peaked in July at 2.4 mm/day and 2.6 mm/day (for a monthly total of 74 mm and 80 mm), respectively for the seismic line and undisturbed area at site U1, compared to 2.3 mm/day and 3.0 mm/day (for a monthly total of 71 mm and 93 mm), respectively for the seismic line and undisturbed area at site L8.

ET values calculated by the Penman-Monteith equation compare well with those simulated by the SHAW model (Fig. 9). Monthly values follow very comparable patterns and annual values are similar. At site U1, annual values are within 6 % for the seismic line and within 15 % for the undisturbed area (Fig. 9A). For this site, the Penman-Monteith equation slightly underestimated ET from May to October. This is likely because the Penman-Monteith equation assumes a uniform grass crop of 0.15 m height (Allen et al., 1998), which is more comparable to the vegetation characteristics (i.e., height, rooting depth) input into the SHAW model on the seismic line than the undisturbed area (see supplementary information, Appendix F, Table F1). For site L8, the simulated ET values are this time always underestimated compared to those calculated by the Penman-Monteith equation, although they remain fairly similar (to within 22 % for the seismic line and within 6 % for the undisturbed area) (Fig. 9B). This underestimation is probably due to the fact that soil was particularly wet in the field, which was could not correctly be reproduced in the model (allowing potential ET to approach actual ET). Overall, the similar ET estimates by the SHAW model and the Penman-Monteith method (Eq. (2)) can be explained by the fact that both rely on the surface energy budget to calculate ET (Scanlon et al., 2002).

The simulated runoff for site U1 was 57.6 mm and 3.8 mm for the seismic line and undisturbed area, respectively (Table 3). Most of this runoff occurred in June following a 52 mm precipitation event (Fig. 9). Conversely, for site L8, runoff estimates were high and similar among the seismic line (240.7 mm) and the undisturbed area (247.6 mm). The large difference in runoff between sites U1 and L8 is mainly due to an extreme rainfall event (the weather station at site L8 measured 146 mm of rain on June 28 and 29, compared to 52 mm at site U1), which accounted for approximately 140 mm of the annual simulated runoff. This extreme event was also recorded by a provincial weather station located near this site (ACIS, 2023). The combination of significant precipitation and spring snow melt resulted in very heavy runoff (170 mm) for the month of June for the seismic line and undisturbed area.

Compared to site U1, the SHAW model predicted approximately 190 mm more runoff over the 12-month period at site L8. This large difference, in addition to the occurrence of the late June extreme rainfall event, can likely be attributed to the different soil and vegetation input parameters used amongst the sites in the simulations, based on available data/observations (see supplementary information, Appendix F, Tables F1 to F3). Indeed, site L8 corresponds to a lowland, hence to wet conditions, which are notorious for poor vegetation recovery (Dabros et al., 2018; Van Rensen et al., 2015) and, moreover, was constructed 19 years after site U1 (Table 1). The overall lower plant canopy cover at site L8 means it is easier for the plant canopy and soil water storage to be overwhelmed and force the model to partition the precipitation into runoff.

Interestingly, in February at site L8, the SHAW model predicted 26 mm and 53 mm of runoff for the seismic line and undisturbed area, respectively, whereas no runoff was predicted at site U1. Recorded weather data indicated the presence of a Chinook wind (warm, generally westerly wind in western North America) as air temperature rose to approximately 4°C and windspeed increased for two days at both sites. However, site L8 had a significantly higher windspeed during this time compared to U1 and thus contributed to approximately 66 mm of snowmelt at L8 (compared to 0 mm at U1), and because the soil was frozen, this was portioned into runoff and evaporation.

Overall, runoff values found by Guarin-Martinez (2022) using a 20-year water budget across the whole 700 km² study area varied between 0 and 151 mm/year. These results are comparable to the SHAW simulations for site U1, whereas site L8 likely provides a maximum (or approaching) value of runoff due to one extreme rain event.

“Deep” percolation (as it is called in the SHAW manual) corresponds to the water flux beyond the deepest soil layer by the SHAW model, which in this case corresponds to 400 cm. Positive values correspond to downward water movement between the two deepest soil layers, whereas negative values indicate upward water movement. This value was considered a proxy for aquifer recharge, as the base of the model is located below the root zone. For sites U1 and L8, a zero value of deep percolation was obtained for the seismic line, whereas 47.8 mm and 21.5 mm of deep percolation were estimated in the adjacent undisturbed area for sites U1 and L8, respectively (Table 3). Deep percolation was greater on the undisturbed areas for both sites likely because of the fieldwork-based soil parameters used (see supplementary information, Appendix F, Tables F2 and F3) in the simulations, such as the lower soil bulk density (see

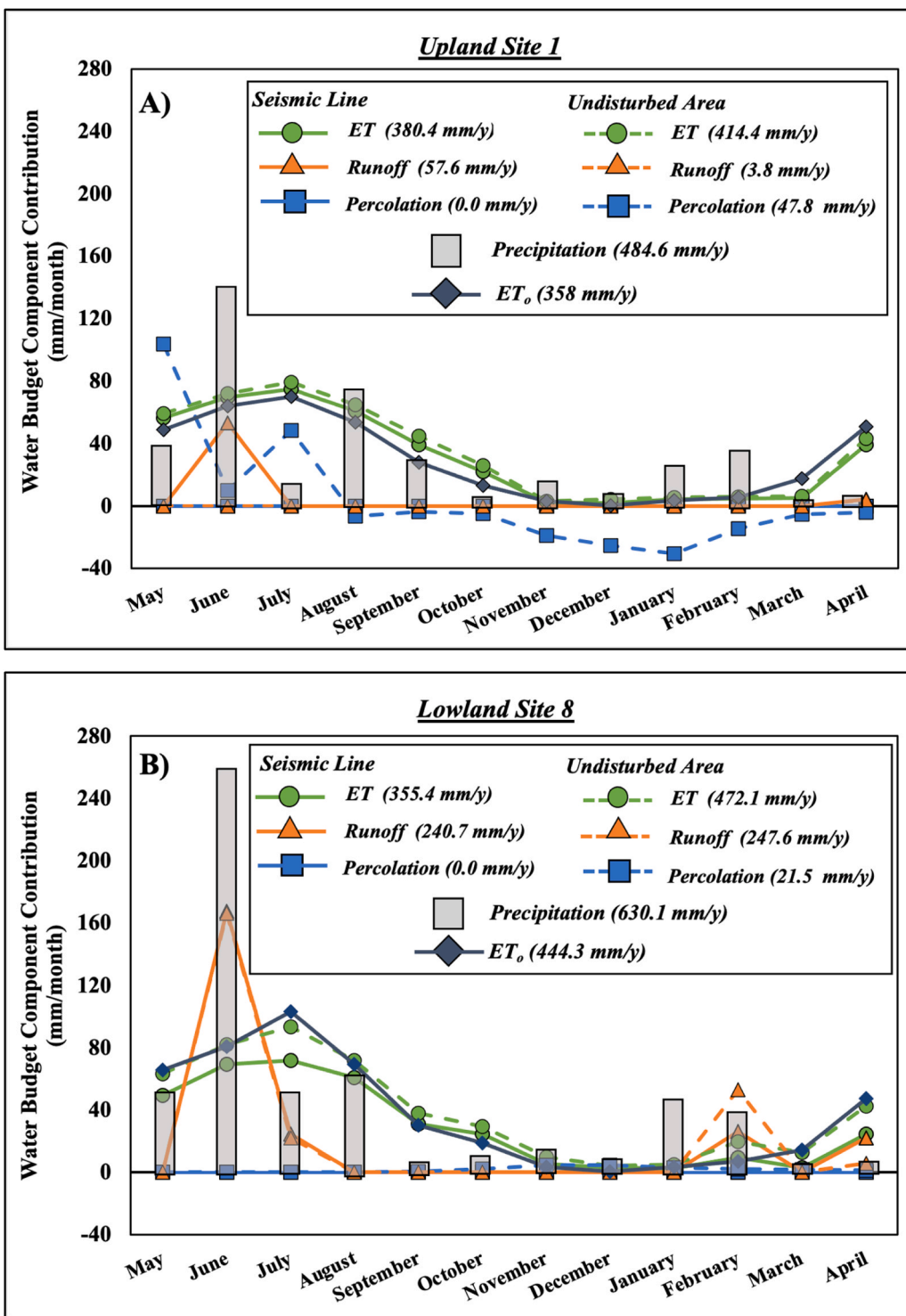


Fig. 9. Primary water budget components (ET, Runoff, and “Deep” Percolation) simulated by the SHAW model and monthly recorded precipitation for A) site U1 and B) site L8 from May 1, 2022, to April 30, 2023. ET_o denotes reference evapotranspiration calculated using the Penman-Monteith (FAO 56) method.

supplementary information, Appendix C, Table C1) compared to their respective seismic lines. This difference increases the water infiltration capacity of the soil and thus the deep percolation estimates by the SHAW model on the undisturbed areas.

Generally, the undisturbed area at U1 had positive or zero monthly deep percolation from April to October when the soil was not

frozen, whereas negative deep percolation values were simulated from November to March when the soil was frozen. Negative deep percolation occurs when the soil profile dries (which is comparable to soil frost formation which causes a drop in SWC) and a fairly moist lower boundary is specified. This results in an upward moisture migration towards the freezing front [pers. commun. with Dr. Flerchinger]. Overall, the deep percolation simulated by the model for both sites are in agreement with the low recharge range (0–70 mm/year) obtained by [Guarin-Martinez \(2022\)](#) for the study area.

The model also outputs a cumulative change in storage value for the soil, snow, residue (i.e., plant litter) and the plant canopy, as well as a cumulative simulation error ([Table 3](#)). A positive change in storage value indicates the amount of water gained whereas a negative value indicates the amount of water used up at the end of the simulation. For instance, the change in water storage for the undisturbed areas of sites U1 and L8 were –12.9 mm and –127.0 mm, respectively, and the seismic lines were 21.8 and –8.6 mm, respectively. The larger negative values on the undisturbed areas reflect a higher plant water demand compared to the seismic lines, and in particular for site L8 the fact that ET in the undisturbed area is largely overestimated due to the use of the weather station of the adjacent seismic line. As noted by [Johnson \(2005\)](#), the water budget components from the SHAW model do not always add up to the total annual precipitation. This is because the soil layers in all simulations begin with an initial water content and that initial soil water will become partitioned throughout the simulation in addition to annual precipitation ([Johnson, 2005](#)) and it is not possible to achieve water balance (i.e. reach steady-state conditions) in a single year. Overall, the cumulative simulation errors calculated by the model were acceptable (< 3 % error) for all sites.

3.5. Water chemistry

3.5.1. Soil water type and pH

Soil water from the upper 1.2 m is dominated by Ca-Mg-HCO₃ ions. Comparatively, groundwater sampled from four shallow (approximately 30 – 35 m deep) wells completed within the Paskapoo aquifer as part of the larger GSC project, revealed one well to contain Ca-HCO₃ type water whereas the other three wells contained Na-HCO₃ type water (i.e., more ‘chemically evolved’) (see [supplementary information](#), Appendix G, Table G1). Water levels in these wells varied between 13 and 24 m from the ground surface. Unsurprisingly, soil water had a lower pH than groundwater.

3.5.2. Precipitation and soil water $\delta^2\text{H}$ and $\delta^{18}\text{O}$ isotopes

Overall, precipitation water isotopes from 2021 to 2022 ranged from a low of –31.6 ‰ for $\delta^{18}\text{O}$ (–240.7 for $\delta^2\text{H}$) in the winter to a high of –13.2 ‰ (–105.9 ‰ for $\delta^2\text{H}$) in the summer ([Fig. 10](#)). The relative snow-water composition of groundwater in this study was estimated to be 40 % using the same method outlined in [Maule et al. \(1994\)](#) (see [supplementary information](#), Appendix H, for its calculation). All soil water samples plotted on or near the LMWL ([Fig. 10](#)) indicating minimal evaporation, a conclusion further supported by lc-excess values, which spanned from –3.3 ‰ to 2.6 ‰ with a median of –0.5 ‰ across 154 soil water samples. No significant differences in $\delta^{18}\text{O}$ and $\delta^2\text{H}$ among the seismic line and undisturbed area were observed. Overall, soil water $\delta^{18}\text{O}$ and $\delta^2\text{H}$ values were generally less variable (decreased standard deviation) and became isotopically enriched with depth ([Fig. 11](#)).

For the ‘shallow samples’ (30 and 60 cm), the most depleted $\delta^{18}\text{O}$ and $\delta^2\text{H}$ values were observed in May following spring melt. In

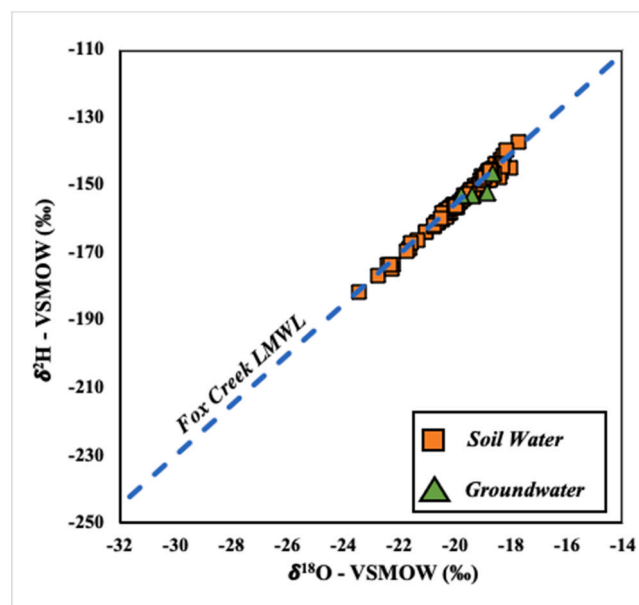


Fig. 10. Dual-isotope plot showing the Fox Creek LMWL, all soil water samples from this study and values from four shallow (approximately 30 m) monitoring wells completed in the Paskapoo Fm. for the larger GSC project.

the following months, seasonal $\delta^{18}\text{O}$ and $\delta^2\text{H}$ values for the shallow soil water had similar median $\delta^{18}\text{O}$ and $\delta^2\text{H}$ values and showed an evolution towards more isotopically enriched values with monthly shifts generally being $< 1\text{‰}$ for $\delta^{18}\text{O}$ (Fig. 11). These monthly shifts are attributed to plant water use that makes room for more meteoric recharge from summer precipitation events and consequently adopting a more isotopically enriched signal. The exception to these trends was site L12 where minimal temporal variation in $\delta^{18}\text{O}$ values was observed at all depths. This is because of the thick peat accumulation at this site which holds a large volume of water; thus, isotopic signatures of individual precipitation events and snowpack melt being likely buffered into an average signal.

Conversely, the deeper samples (120 cm) had a relatively consistent isotopic signature with a median of -18.8 (± 0.2) ‰ (near analytical error ($< 0.15\text{‰}$) and -147.5 (± 1.7) ‰ for $\delta^{18}\text{O}$ and $\delta^2\text{H}$, respectively). These values are comparable to $\delta^{18}\text{O}$ and $\delta^2\text{H}$ values from limited ($n = 4$) shallow (32–35 m well depths) groundwater samples from the Paskapoo aquifer obtained from nearby monitoring wells: -19.0 (± 0.4) ‰ and -150.6 (± 3.4) ‰ for $\delta^{18}\text{O}$ and $\delta^2\text{H}$, respectively.

An exception to the reduced temporal variation in $\delta^{18}\text{O}$ and $\delta^2\text{H}$ values with depth is site U1, particularly on the seismic line. At this site, the monthly variations at 120 cm were closer to those of shallow soil water, indicating that meteoric water can consistently infiltrate to this depth at this site (unlike the other sites). This could result from several reasons, including that the soil at 120 cm has a better hydraulic connection with the shallow soil layers than at the other sites due to the presence of preferential flow paths.

4. Discussion

4.1. Impacts of seismic lines

The unique footprint of a seismic line implies that the water budget components are unlikely to remain unchanged after disturbance. Indeed, following natural disturbances (e.g., forest fires, pests), boreal ecosystems typically begin to regenerate in the following growing season and evolve through the various successional stages towards the pre-disturbance state (Dabros et al., 2018). In comparison, seismic lines often do not follow such a successional trajectory, but rather remain in the early successional stages (Van Rensen et al., 2015) and therefore have no natural analogue (Dabros et al., 2018). Van Rensen et al., (2015) predicted that following 50 years post-disturbance, approximately one-third of existing linear disturbance footprints in this boreal landscape will remain unregenerated in the boreal landscape. For instance, Lee and Boutin (2006) observed that wide seismic lines (thus, pre-2000) only partially recovered in upland aspen and white spruce forests and lowland black spruce forests. They found that following a significant time lag (35 years), upland ecoregions were more likely to recover to $> 50\%$ woody vegetation compared to wet lowland black spruce forests, which showed minimal to no recovery. However, it should be noted that although upland seismic lines were more likely to regenerate, most (approximately 65 % in their study) showed minimal regeneration other than a cover of low-growing forbs.

The results from the SHAW model and field measurements (including SWC and temperature datasets) suggest that seismic line

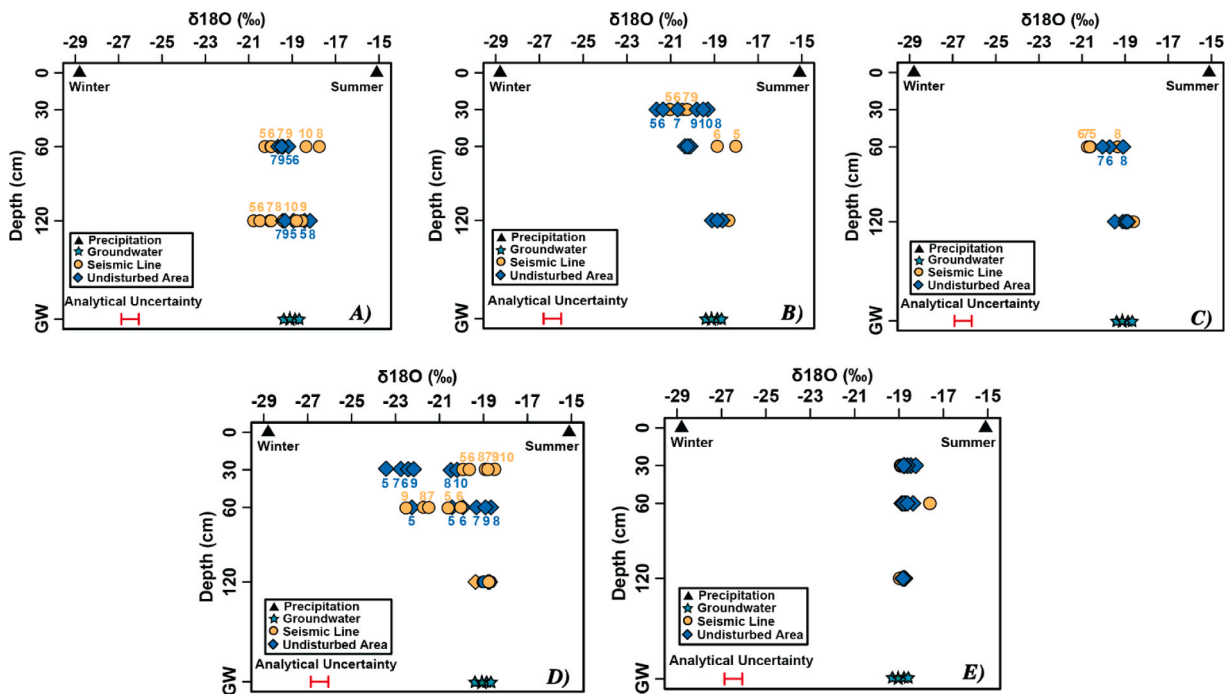


Fig. 11. Seasonal variations in $\delta^{18}\text{O}$ values at A) U2 B) L8 and C) L12 separated by depth in the study area (numbers above points indicate month of the year). Shown for reference are shallow (approximately 30 m) Paskapoo groundwater $\delta^{18}\text{O}$ values (\pm standard deviation) along with average winter and summer precipitation $\delta^{18}\text{O}$ values. GW denotes groundwater.

construction may result in decreased ET and canopy interception due to reduced vegetation cover, and potentially negative impacts on soil dynamics (e.g., soil moisture), which promote enhanced runoff and therefore less infiltration. However, the effects of seismic lines on the water budget components largely depend on local site conditions. Generally, the post-disturbance hydrologic response of a landscape impacted by seismic lines will depend on the seismic line width and orientation, height of the adjacent canopy (shading), seasonality, degree of vegetation recovery, level of initial disturbance, variations in microtopography and reuse frequency of the seismic line. In the study area, seismic lines account for 61 % of all linear disturbances (Le et al., 2023), which appears to be significantly higher than the seismic line abundance estimated for a large part of the Canadian boreal forest, representing 46 % of all linear features (Pasher et al., 2013). Nonetheless, the high density and prevalence of seismic lines in the Canadian boreal forest means their impact on the hydrologic functioning of a landscape cannot be ignored. This becomes especially significant given that there are currently no reclamation requirements for seismic lines and that anthropogenic disturbances in general are expected to increase in western Canada (Dabros et al., 2018).

4.2. Soil water content

Interestingly, SWC was not consistently greater on the seismic lines and varied amongst the depths and time of measurement at each study site. For study sites with a similar soil texture (U1, U2, U3, and L12 primarily), the SWC tended to be higher at shallower depths (15 and 30 cm) on the undisturbed area from June to August (Figs. 4 to 6). This is somewhat counterintuitive as one might expect the decreased canopy cover on seismic lines to result in an increased SWC, particularly during the growing season which is when most (65–75 %) of annual precipitation occurs in the BP (Devito et al., 2012). However, the higher windspeed and net solar radiation on the seismic line likely contribute to increased soil water evaporation, and thus drier conditions on the seismic line relative to the adjacent undisturbed area. Additionally, the higher SOM content in the surface soil layers on the undisturbed areas (see [supplementary information](#), Appendix C, Table C1), contributes to a greater water retention.

Other studies measuring SWC on seismic lines have shown conflicting results. For example, Weiland et al. (2023) measured SWC on an EW oriented seismic line in Fort McMurray. While they found that at 5 cm depth, SWC was consistently greater on the seismic line, at 15 and 25 cm depths, SWC was consistently greater on the undisturbed area, as observed in this study. Dabros et al. (2017) collected SWC data on narrow (3–5 m wide), EW oriented seismic lines in mature upland black spruce-lodgepole pine dominated forests in Swan Hills AB. They found that seismic lines had a consistently higher SWC compared to the undisturbed area at 12 cm. Similarly, Davidson et al. (2020) observed a higher SWC at 10 cm on wide (5 – 10 m) seismic lines in treed fen and poor mesic sites in Fort McMurray AB. These conflicting results likely arise from local site conditions relating to the characteristics of the seismic lines.

4.3. Changes in the water budget components

4.3.1. Evapotranspiration

Generally, forest cover loss results in ET to decline for two reasons: (i) the clearing of vegetation results in decreased transpiration and (ii) the reduced vegetation cover leads to less intercepted precipitation and more wind, both of which can reduce the snow cover, leading to a decrease in sublimation (snow) and/or water available for evaporation (rain) back to the atmosphere (Goeking and Tarboton, 2020). The substantial lag in regeneration thus contributes to an overall decrease in ET on seismic lines.

The results from this study are in line with the findings from Lee and Boutin (2006) that upland sites are more likely to regenerate than lowland sites from two perspectives. Firstly, the upland seismic line and undisturbed area exhibited a higher and more comparable peak LAI (in August) compared to the lowland site (see [supplementary information](#), Appendix B, Table B2). Secondly, the percent cover vegetation data (see [supplementary information](#), Appendix B, Figures B1 and B2) and tree height data (see [supplementary information](#), Appendix B, Table B1) indicated that the upland study sites had a greater degree of woody vegetation recovery and taller trees on the seismic lines compared to the lowland black spruce sites. As these vegetation data were used as input parameters in the SHAW model, the model predicted a smaller difference in ET on the seismic line of the upland site (94.2 mm) compared to the lowland site (116.8 mm).

4.3.2. Runoff

The results of this study showed that BD measurements from the upper 15 cm of the soil-profile were higher by 8–65 % on the seismic lines of all study sites compared to the undisturbed sites, potentially indicating some compaction. However, a higher BD has not always been observed on seismic lines. For instance, for upland sites to the north of the study area, Filicetti and Nielsen (2022) found significantly ($p < 0.001$) higher BD values for the upper 20 cm of soil on seismic lines (0.67 g/cm^3 ($n = 146$)) compared to their respective adjacent undisturbed areas (0.50 g/cm^3 ($n = 146$)), whereas Van Dongen et al. (2023) found no statistically significant differences ($p = 0.61$) in BD for the upper 15–20 cm of disturbed soil. The larger difference in BD among the seismic line and undisturbed area at site U1 compared to L8 (see [supplementary information](#), Appendix C, Table C1) contributed to an increased runoff in the SHAW model on the seismic line at site U1 (53.8 mm/y) compared to the undisturbed area, whereas at L8 runoff simulations were high yet similar (approximately 240 mm/y), but this was mainly due to the extreme rain event. The variations in BD among sites can again be attributed to many factors: (i) soil-texture type, (ii) recent re-use of seismic lines (e.g., recreational and/or animal use) (iii) ecosite type and its associated soils (e.g., texture, SOM content), (iv) degree of vegetation cover (Dabros et al., 2018; Davidson et al., 2020; Filicetti and Nielsen, 2022).

4.3.3. Infiltration

Groundwater recharge in the BP derives mainly from spring snowmelt, whereas recharge is relatively low during the growing season apart from larger rainfall events (Smerdon et al., 2008; Redding and Devito, 2011; Thompson et al., 2017). The $\delta^{18}\text{O}$ and $\delta^2\text{H}$ isotope data from precipitation and groundwater in this study corroborated this observation. Indeed, this is evidenced by the average isotopic signature of groundwater from the shallow monitoring wells in the study area (-20.0 ‰ for $\delta^{18}\text{O}$), which was slightly lower than the median annual precipitation value (-19.4 ‰ for $\delta^{18}\text{O}$). The lower $\delta^{18}\text{O}$ values found in the shallow groundwater systems within the study area are thought to be representative of recent precipitation water (Rivard et al., 2023), based on the geochemical data for this study area. This is precisely the case for this study and not unusual for this region: this conclusion has been reported in many other studies of groundwater recharge in Alberta (Fritz and Krouse, 1973; Hendry, 1988; Maule et al., 1994). The high snow water contribution to the groundwater likely results from snowmelt runoff that percolates into nearby shallow depressions and/or sandier areas, resulting in local recharge to the water table.

Interestingly, the low temporal variation in $\delta^{18}\text{O}$ and $\delta^2\text{H}$ values for the 'deep' (120 cm) soil water at most study sites (except for site U1) in this study appear to largely confine meteoric recharge between 60 and 120 cm following spring melt. This may be related to the high content of fine particles in soils (typically > 70 %, Rivard et al., 2023) that does not favor infiltration. Additionally, the ratio of P to ET close to 1 (as supported by the weather data and SHAW simulations in this study) means that little excess water is available and that interannual climate variations (such as extreme rainfall events) can play a major role in the water budget. As previously mentioned, the exception to this was at site U1 (Fig. 11), whose isotopic values indicate recharge beyond 120 cm suggesting the presence of local preferential recharge flow paths. Further analysis would be required to better understand groundwater recharge processes in this study area.

4.4. Further impacts of climate change

Human disturbances in North America over the past several decades have led to a general trend towards higher mean and extreme temperatures (IPCC, 2023). Ecosystems within the BP are particularly sensitive to increasing temperatures because of the long-term water deficit in the region posed by the close relationship between precipitation and ET (Devito et al., 2012; Thompson et al., 2017). By 2050, temperatures within the BP are expected to increase further by 2–5 °C (Hayhoe and Stoner, 2019). More specifically, in Alberta, winter temperatures are projected to rise by 2 °C and summer temperatures by 1.5 °C for each 1 °C increase in global temperatures (Hayhoe and Stoner, 2019). These warmer projected temperatures in the BP will lead to warmer spring and fall temperatures and thus the lengthening of the growing season (Brown et al., 2010; Devito et al., 2012; Thompson et al., 2017), which would likely increase current ET and in turn affect the other water budget components. Although annual precipitation in the BP is expected to increase by the 2050s, future estimates are highly uncertain, and in Alberta, minimal changes in average annual precipitation are expected (Hayhoe and Stoner, 2019). Nonetheless, changes in precipitation patterns are predicted to result from climate change, increasing the occurrence of extreme events (IPCC, 2023) and non-negligible seasonal, rather than annual, changes in the values of water balance components are expected (e.g. annual recharge may remain fairly stable due to possible winter recharge episodes while spring and summer recharge would be reduced, thereby decreasing the amount of water available for streams and vegetation) (Rivard et al., 2009).

Among the predicted changes in the BP, upland forests will become increasingly water stressed as the growing season will lengthen leading to depleted soil water stocks (Hogg et al., 2002; Schneider et al., 2016; Thompson et al., 2017). The effects of this have already been observed in recent years across widespread areas of Western and Eastern Canada, which have experienced aspen forest mortality (Thompson et al., 2017), as well as the devastating large-scale forest fires of summer 2023. Considering this, future climate modeling shows that the climate may become unsuitable for aspen stands in the western BP (Bergengren et al., 2011; Worrall et al., 2013), and thus a northward migration of prairie grasslands may occur (Hogg and Hurdle, 1995; Bergengren et al., 2011). In the context of linear disturbances that include seismic lines, the literature on future climate modeling suggests that the combined effects of reduced competition due to aspen mortality and ongoing climate change may lead to major changes in species (Schneider et al., 2003; 2016). On the other hand, modeling for peatlands has predicted that water levels would be resistant and resilient to changing climate (Waddington et al., 2015; Thompson et al., 2017). While the fact that peatlands may sustain their moisture regime is very positive, it also means that the seismic lines created on these ecosystems are unlikely to regenerate in the near future, based on the work by Van Rensen et al., (2015) who observed minimal to no regeneration after 50 years in a region to the northeast of our study area.

4.5. Study limitations and future research

The water budget analysis established using the SHAW model, which simulates a large number of processes, but requires numerous input data to do so, used several assumptions that may lead to a large degree of uncertainty within the model results. For instance, to better understand water movement in the critical zone, and in particular deep percolation in the unsaturated zone, additional soil data (e.g., particle size index, saturated hydraulic conductivity, and air entry potential) should be collected rather than relying on estimates provided using empirical equations.

Furthermore, the results of this study (and in particular of the SHAW model) would benefit from a multi-year dataset and the characterization of additional sites, which would help validate the current results, improve model calibration, reduce uncertainty for certain parameters and thereby of the model response, and finally obtain a range for water budget components for drier and wetter years. It would also be interesting to extend the SHAW model (down to a few meters) to see whether the water budget values change. However, these recommendations are idealistic and may not be feasible, as they would involve considerable fieldwork, which is very

time-consuming and costly. This study involved monthly field campaigns over 1.5 years and the deployment of a large number of sensors and instruments/stations. In addition, the installation of deeper sensors and equipment would require the use of mechanized equipment, whereas all installations in this study were performed manually. For sites located quite far from roads, this would pose some challenges.

Additionally, although the SHAW model can take into account a multi-species plant canopy, it treats each species as a homogeneous stand (i.e., with the same height). However, tree and shrub regeneration on seismic lines is not homogeneous, but rather complicated and depends on a multitude of factors: seismic line characteristics (width, length, aspect), disturbance history, subsequent anthropogenic activities and ecosite type (Dabros et al., 2018; Lee and Boutin, 2006; Van Rensen et al., 2015). The seismic lines analyzed in this study were constructed in different years (Table 1). As a result, they are currently at varying stages of recovery, which could impact the data input into the model. This variability could therefore introduce additional uncertainty into the results. Moreover, the overall effects of seismic lines on the hydrology are likely underestimated because of edge effects (i.e., the difference in a response variable between the seismic line-forest edge and the forest interior) (Dabros et al., 2018), which were not considered in this study. Further studies could contribute to the development of a spatial (2D or 3D) model that would allow for the characteristics of the numerous seismic lines and other disturbance to be considered and a more comprehensive understanding of the broader landscape effects.

While this study, along with others (Braverman and Quinton, 2016; Dabros et al., 2018), demonstrate that seismic lines do influence the local hydrology of an area, their regional impacts remain undefined. However, we can probably speculate that the regional hydrological effects of seismic lines and other infrastructure may be important in areas with extensive industrial activities, such as the boreal ecosystems of North America, where seismic lines are ubiquitous and widespread. For instance, Timoney and Lee (2001) estimated a total length of up to 1.8 million km of lines in Alberta alone. The abundance of seismic lines in such regions, and the pipelines, roads and O&G well pads that usually accompany them, could cause hydrological changes that amplify or offset one another and cumulatively lead to varied effects on larger spatial scales. Indeed, landscape change modifies the interactions between different environmental components (vegetation, soil and atmosphere), altering hydrological dynamics. This lack of knowledge highlights the urgent need for further investigation into their cumulative effect at a larger scale.

Based on the results of our study, although limited, it seems reasonable to hypothesize that the considerable forest fragmentation due to industrial activities throughout the 700 km² study area (36 % forest loss, with seismic lines accounting for 61 % of all linear disturbances (Le et al., 2023)), could have important regional implications for the hydrology of this region. Indeed, the two contrasted modeled ecosites both showed a reduction in ET and percolation on the seismic line compared to the undisturbed adjacent forest, suggesting that these results could possibly be transposed to the watershed scale. However, further research is required to evaluate the regional hydrological impacts of infrastructure and the main factors affecting them.

5. Conclusions

This study investigated the impacts of seismic lines on hydrological processes for five paired study sites, and in more detail for two of them, located in a ~700 km² watershed near the town of Fox Creek (west-central Alberta, western Canada), a region highly fragmented due to intensive activities by the forest and especially the O&G industry. To achieve this, intensive fieldwork was carried out to collect data on weather, soil texture, soil water content, temperature and geochemistry, and a local meteoric line. These data were then integrated into a 1D hydrological model that takes into account vegetation and soil characteristics, as well as snow/ice freeze/thaw cycles.

Weather data on seismic lines indicated an increased air temperature, windspeed, and net solar radiation compared to the adjacent undisturbed areas. However, as seismic lines have reduced vegetation compared to undisturbed areas (due to slow and sometimes difficult vegetation recovery), ET is in many cases reduced. Isotopic water data ($\delta^{18}\text{O}$ and $\delta^2\text{H}$) of soil water indicate that significant percolation only occurs in the upper 60 cm of soil, except at one site, confirming that aquifer recharge in this area occurs through local preferential flow.

Although common findings can be found from the soil water content (SWC) and temperature datasets (e.g., on seismic lines, spring thaw often occurs earlier and summer temperature is always higher due to reduced canopy than on undisturbed areas), what emerges from this study is that it is difficult to draw general conclusions despite the efforts made to equip sites to characterize, measure and monitor several parameters in the critical zone due to the complexity of the processes at play arising from site-specific characteristics and conditions.

Nonetheless, the SHAW model predicted an annual reduction in ET on the seismic lines at the two modeled ecosites (sites U1 and L8) by 33 % and 9 %, respectively. Runoff estimates were higher on the seismic line of the upland site by 54 mm and comparable at site L8. These results suggest that seismic lines change the water dynamics in the critical zone and the degree to which hydrological processes are altered is determined by local site conditions. Given that 1) a significant percentage of Canada's boreal forest is affected by forest cutting (by different industries, including O&G and logging) and thus landscape fragmentation (36 % in our study area) and 2) climate change is expected to bring warmer conditions and water stress due to the lengthening of the growing season, particularly in the uplands, the results of this study should raise concerns and encourage further studies to be carried out. A better understanding of the impacts of industrial activities in this region and elsewhere, in order to support the development of new legislation, will help to better protect these fragile, yet ecologically important forest environments.

CRedit authorship contribution statement

Kelly J. Rozanitis: Resources, Investigation. **Baptiste Coutret:** Resources, Investigation. **Kurt O. Konhauser:** Resources, Funding

acquisition. **Daniel S. Alessi**: Writing – review & editing, Supervision, Project administration, Funding acquisition. **Daniels Kononovs**: Writing – original draft, Investigation, Formal analysis, Data curation. **Christine Rivard**: Writing – review & editing, Supervision, Project administration, Funding acquisition. **Dani Degenhardt**: Writing – review & editing, Supervision, Project administration, Funding acquisition. **Katherine N. Snihur**: Writing – review & editing, Resources, Investigation. **Daniela Gutierrez-Rueda**: Resources, Investigation. **Cody N. Lazowski**: Resources, Investigation.

Declaration of Competing Interest

The authors declare that they have no known competing financial interests or personal relationships that could have appeared to influence the work reported in this paper.

Acknowledgments

This research was made possible through research funding provided by the Geological Survey of Canada of Natural Resources Canada and a Natural Sciences and Engineering Research Council of Canada (NSERC) Discovery Grant to DSA (RGPIN-2020–05289). We would like to thank Kaitlyn Trepanier and Caren Jones (Northern Forestry Centre, Canadian Forest Service, Natural Resources Canada). We also would like to acknowledge Dr. Miles Dyck for providing lysimeters used in this study.

Appendix A. Supporting information

Supplementary data associated with this article can be found in the online version at [doi:10.1016/j.ejrh.2024.102133](https://doi.org/10.1016/j.ejrh.2024.102133).

Data availability

Data will be made available on request.

References

- ACIS, 2023. Alberta Climate Information Service: Agriculture and Irrigation. Hydrocarbon Resources in Alberta. <https://acis.alberta.ca>. Accessed 18 Nov 2023..
- AER, 2023. Low Permeability and Shale Area Assessment – Duvernay Formation. In: Alberta Energy Regulator. <https://www.aer.ca/providing-information/data-and-reports/statistical-reports/st98/reserves/low-permeability-and-shale-area-assessment/reserves-duvernay-formation>. Accessed 7 Feb 2024..
- AGS, 2023. Hydrocarbon Resources in Alberta. <https://ags.aer.ca/research-initiatives/oil-and-gas>. Accessed 18 Oct 2023..
- Allen, R.G., Pereira, L.S., 2009. Estimating crop coefficients from fraction of ground cover and height. *Irrig. Sci.* 28, 17–34. <https://doi.org/10.1007/s00271-009-0182-z>.
- Allen, R.G., Pereira, L.S., Raes, D., Smith, M., 1998. *Crop Evapotranspiration: Guidelines for Computing Crop Water Requirements*. Food and Agriculture Organization of the United Nations, Rome.
- Allen, R.G., Pereira, L.S., Howell, T.A., Jensen, M.E., 2011. Evapotranspiration information reporting: I. Factors governing measurement accuracy. *Agric. Water Manag.* 98, 899–920. <https://doi.org/10.1016/j.agwat.2010.12.015>.
- Atkinson, L.A., Hartman, G.M.D., 2017. AER/AGS Report 93: 3D Rendering of the Regional Stratigraphy of Paleogene–Quaternary Sediments in West-Central Alberta. *Alta. Energy Regul. /Alta. Geol. Surv. Rep.* 93, 51.
- Beckingham, J.D., Archibald, J.H., 1996. *Field Guide to Ecosites of Northern Alberta*. Northern Forestry Center.
- Bergengren, J.C., Waliser, D.E., Yung, Y.L., 2011. Ecological sensitivity: a biospheric view of climate change. *Clim. Change* 107, 433–457. <https://doi.org/10.1007/s10584-011-0065-1>.
- Betts, A.K., Ball, J.H., 1997. Albedo over the boreal forest. *J. Geophys Res* 102, 28901–28909. <https://doi.org/10.1029/96JD03876>.
- Bliss, L.C., Wein, R.W., 1972. Plant community responses to disturbances in the western Canadian Arctic. *Can. J. Bot.* 50, 1097–1109. <https://doi.org/10.1139/b72-136>.
- Brantley, S.L., Goldhaber, M.B., Ragnarsdottir, K.V., 2007. Crossing Disciplines and Scales to Understand the Critical Zone. *Elements* 3, 307–314. <https://doi.org/10.2113/gselements.3.5.307>.
- Braverman, M., Quinton, W.L., 2016. Hydrological impacts of seismic lines in the wetland-dominated zone of thawing, discontinuous permafrost, Northwest Territories, Canada. *Hydrol. Process.* 30, 2617–2627. <https://doi.org/10.1002/hyp.10695>.
- Brown, S., Biswas, A., Caron, J., Dyck, M., 2021. Soil Physics. In: Krzic, In.M., Walley, F.L., Diochan, A., Pare, M.C., Farrell, R.E. (Eds.), *Digging into Canadian Soils: An introduction to soil science*. Canadian Society of Soil Science, Pinawa, M.B., pp. 100–149 (<https://openpress.usask.ca/soilscience/chapter/soil-health-and-management/>).
- Brown, S.M., Petrone, R.M., Mendoza, C., Devito, K.J., 2010. Surface vegetation controls on evapotranspiration from a sub-humid Western Boreal Plain wetland. *Hydrol. Process.* 24, 1072–1085. <https://doi.org/10.1002/hyp.7569>.
- Caplan, J.S., Yeakley, J.A., 2010. Water relations advantages for invasive *Rubus armeniacus* over two native ruderal congeners. *Plant Ecol.* 210, 169–179. <https://doi.org/10.1007/s11258-010-9747-4>.
- Craig, H., 1961. Isotopic variations in meteoric waters. *Science* 133, 1702–1703. <https://doi.org/10.1126/science.133.3465.1702>.
- Dabros, A., Hammond, H.E.J., Pinzon, J., Pinno, B.D., Langor, D.W., 2017. Edge influence of low-impact seismic lines for oil exploration on upland forest vegetation in northern Alberta (Canada). *For. Ecol. Manag.* 400 (2017), 278–288. <https://doi.org/10.1016/j.foreco.2017.06.030>.
- Dabros, A., Pyper, M., Castilla, G., 2018. Seismic lines in the boreal and arctic ecosystems of North America: environmental impacts, challenges, and opportunities. *Environ. Rev.* 26, 214–229. <https://doi.org/10.1139/er-2017-0080>.
- Davidson, S.J., Goud, E.M., Franklin, C., Nielsen, S.E., Strack, M., 2020. Seismic line disturbance alters soil physical and chemical properties across boreal forest and peatland soils. *Front Earth Sci.* 8. <https://doi.org/10.3389/feart.2020.00281>.
- Devito, K., Mendoza, C., Qualizza, C., 2012. Conceptualizing water movement in the Boreal Plains. Implications for watershed reconstruction. Synthesis report prepared for the Canadian Oil Sands Network for Research and Development. Environmental and Reclamation Research Group.
- FAO, 2012. ETo Calculator. Land and Water Digital Media Series. Food and Agriculture Organization (FAO). Rome, Italy (<https://www.fao.org/nr/water/ETo.html>).

- Filicetti, A.T., Nielsen, S.E., 2022. Effects of wildfire and soil compaction on recovery of narrow linear disturbances in upland mesic boreal forests. *For. Ecol. Manag.* 510, 120073. <https://doi.org/10.1016/j.foreco.2022.120073>.
- Flerchinger, G.N., 2017b. Simultaneous Heat and Water (SHAW) Model: Use 'S. Man. Version 3. 0. x.
- Flerchinger, G.N., 2017a. The Simultaneous Heat and Water (SHAW) Model. *Tech. Doc.* 3 (0).
- Flerchinger, G.N., Hardegree, S.P., 2004. Modelling near-surface soil temperature and moisture for germination response predictions of post-wildfire seedbeds. *J. Arid Environ.* 59, 369–385. <https://doi.org/10.1016/j.jaridenv.2004.01.016>.
- Flerchinger, G.N., Pierson, F.B., 1991. Modeling plant canopy effects on variability of soil temperature and water. *Agric. For. Meteorol.* 56, 227–246. [https://doi.org/10.1016/0168-1923\(91\)90093-6](https://doi.org/10.1016/0168-1923(91)90093-6).
- Flerchinger, G.N., Saxton, K.E., 1989. Simultaneous heat and water model of freezing snow-residue-oil system I theory and development. *Trans. Am. Soc. Agric. Eng.* 32, 565–571.
- Flerchinger, G.N., Caldwell, T.G., Cho, J., Hardegree, S.P., 2012. Simultaneous Heat and Water (SHAW) Model: Model Use, Calibration, and Validation. *Trans. ASABE* 55, 1395–1411. <https://doi.org/10.13031/2013.42250>.
- Flinn, M.A., Wein, R.W., 1977. Depth of underground plant organs and theoretical survival during fire. *Can. J. Bot.* 55, 2550–2554.
- Fox Creek Historical Association, 1992. Iosegun Reflections: A History of Fox Creek. Fox Creek Historical Association.
- Fritz, P., Krouse, H.R., 1973. Wabamun Lake past and present: an isotopic study of the water budget. In: *Proceedings of Symposium on Lakes of Western Canada, 2*. University of Alberta, Water Resources Center, Edmonton, pp. 244–256.
- Gauthier, S., Bernier, P., Kuuluvainen, T., Shvidenko, A.Z., Schepaschenko, D.G., 2015. Boreal forest health and global change. *Science* 349, 819–822. <https://doi.org/10.1126/science.aaa9092>.
- Goeking, S.A., Tarboton, D.G., 2020. Forests and Water Yield: A Synthesis of Disturbance Effects on Streamflow and Snowpack in Western Coniferous Forests. *J. For.* 118, 172–192. <https://doi.org/10.1093/jofore/fvz069>.
- Gosselin, J.S., Rivard, C., Martel, R., Lefebvre, R., 2016. Application limits of the interpretation of near-surface temperature time series to assess groundwater recharge. *J. Hydrol.* 538, 96–108.
- Green, I.R.A., Stephenson, D., 1986. Criteria for comparison of single event models. *Hydrol. Sci. J.* 31, 395–411.
- Green, W.H., Ampt, G., 1911. Studies on soil physics. *J. Agric. Sci.* 4, 1–24.
- Gröning, M., Lutz, H.O., Roller-Lutz, Z., Kralik, M., Gourcy, L., Pöntenstein, L., 2012. A simple rain collector preventing water re-evaporation dedicated for δ18O and δ2H analysis of cumulative precipitation samples. *J. Hydrol.* 448, 195–200. <https://doi.org/10.1016/j.jhydrol.2012.04.041>.
- Guarin-Martinez, L.I., 2022. Characterization and Numerical Modeling of the Bedrock Aquifer in the Fox Creek Area, Alberta. *Maîtrise En. Sci. De. la Terre, Univ. é du Québec*.
- Hayhoe, K., Stoner, A., 2019. *Alta. 'S. Clim. Future.: Final Rep. 2019. ATMOS Res. Consult.*
- Hébert, F., Thiffault, N., 2011. The Biology of Canadian Weeds. 146. *Rhododendron groenlandicum* (Oeder) Kron and Judd. *Can. J. Plant Sci.* 91, 725–738. <https://doi.org/10.4141/cjps2010-012>.
- Hendry, M.J., 1988. Hydrogeology of Clay Till in a Prairie Region of Canada. *Groundwater* 26, 607–614. <https://doi.org/10.1111/j.1745-6584.1988.tb00794.x>.
- Hogg, E.H., Hurdle, P.A., 1995. The aspen parkland in western Canada: A dry-climate analogue for the future boreal forest? *Can. For. Serv.*
- Hogg, E.H., Brandt, J.P., Kochtubajda, B., 2002. Growth and dieback of aspen forests in northwestern Alberta, Canada, in relation to climate and insects. *Can. J. Res* 32, 823–832. <https://doi.org/10.1139/x01-152>.
- Huang, M., Gallichand, J., 2006. Use of the SHAW model to assess soil water recovery after apple trees in the gully region of the Loess Plateau, China. *Agric. Water Manag.* 85, 67–76. <https://doi.org/10.1016/j.agwat.2006.03.009>.
- Hughes, A.T., Smerdon, B.D., Alessi, D.S., 2017. Hydraulic properties of the Paskapoo Formation in west-central Alberta. *Can. J. Earth Sci.* 54, 883–892. <https://doi.org/10.1139/cjes-2016-0164>.
- IPCC, 2023. *Climate Change 2022 – Impacts, Adaptation and Vulnerability: Working Group II Contribution to the Sixth Assessment Report of the Intergovernmental Panel on Climate Change, 1st edn.* Cambridge University Press.
- Islam, Z., 2013. Evaporation and Evapotranspiration: Methods and Application Alberta. <https://doi.org/10.13140/RG.2.1.2730.0249>.
- Johnson, A.R., 2005. Assessing the Performance of a Salix-based evapotranspiration (ET) Cover using the SHAW Model. Master's Thesis, State University of New York, College of Environmental Science and Forestry, Syracuse, New York.
- Kalra, Y.P., Maynard, D.G., 1991. *Manual for Forest Soil and Plant Analysis.* Forestry Canada, Northwest Region.
- Kang, E., Cheng, G., Song, K., Jin, B., Liu, X., Wang, J., 2005. Simulation of energy and water balance in Soil-Vegetation-Atmosphere Transfer system in the mountain area of Heihe River Basin at Hexi Corridor of northwest China. *Sci. China Ser. D. -Earth Sci.* 48, 538–548. <https://doi.org/10.1360/02yd0428>.
- Kaufmann, M.R., 1975. Leaf water stress in engelmann spruce: influence of the root and shoot environments. *Plant Physiol.* 56, 841–844. <https://doi.org/10.1104/pp.56.6.841>.
- Knapik, L.J., Lindsay, J.D., 1983. Reconnaissance Soil Surv. Iosegun Lake Area, Alta.
- Kononovs, D., 2023. Characterizing the Impacts of Seismic Exploration Lines on the Hydrology and Vadose Zone for a Watershed in West-Central Alberta. Master's Thesis. University of Alberta, Department of Earth and Atmospheric Sciences. Edmonton, Alberta.
- Le, B.T., Ha, T., Darling, S., Xu, B., 2023. Historical land use changes and lichen-rich ecosystems near Fox Creek, Alberta. *Geological survey of Canada* <https://soi.org/10.4095/332152>.
- Lee, P., Boutin, S., 2006. Persistence and developmental transition of wide seismic lines in the western Boreal Plains of Canada. *J. Environ. Manag.* 78, 240–250. <https://doi.org/10.1016/j.jenvman.2005.03.016>.
- Link, T.E., Flerchinger, G.N., Unsworth, M., Marks, D., 2004. Simulation of Water and Energy Fluxes in an Old-Growth Seasonal Temperate Rain Forest Using the Simultaneous Heat and Water (SHAW) Model. *J. Hydrometeorol* 5, 443–457. [https://doi.org/10.1175/1525-7541\(2004\)005<0443:SOWAEF>2.0.CO;2](https://doi.org/10.1175/1525-7541(2004)005<0443:SOWAEF>2.0.CO;2).
- Liu, C., Sun, G., McNulty, S.G., Noormets, A., Fang, Y., 2017. Environmental controls on seasonal ecosystem evapotranspiration/potential evapotranspiration ratio as determined by the global eddy flux measurements. *Hydrol. Earth Syst. Sci.* 21, 311–322. <https://doi.org/10.5194/hess-21-311-2017>.
- Lyster, S., Andriashek, L.D., 2012. Geostatistical Rendering of the Architecture of Hydrostratigraphic Units within the Paskapoo Formation. *Cent. Alta.* 115.
- Maule, C.P., Chanasyk, D.S., Muehlenbachs, K., 1994. Isotopic determination of snow-water contribution to soil water and groundwater. *J. Hydrol.* 155, 73–91. [https://doi.org/10.1016/0022-1694\(94\)90159-7](https://doi.org/10.1016/0022-1694(94)90159-7).
- McNamara, J.P., Chandler, D., Seyfried, M., Achet, S., 2005. Soil moisture states, lateral flow, and streamflow generation in a semi-arid, snowmelt-driven catchment. *Hydrol. Process* 19, 4023–4038. <https://doi.org/10.1002/hyp.5869>.
- Monteith, J.L., 1965. Evaporation and environment. In: *Symposium of the Society for Experimental Biology*, 19. Cambridge University Press, pp. 205–234.
- Nash, J.E., Sutcliffe, J.V., 1970. River flow forecasting through conceptual models: Part 1 - a discussion of principles. *J. Hydrol.* 44 282–290.
- Pasher, J., Seed, E., Duffe, J., 2013. Development of boreal ecosystem anthropogenic disturbance layers for Canada based on 2008 to 2010 Landsat imagery. *Can. J. Remote Sens.* 39, 42–58. <https://doi.org/10.5589/m13-007>.
- Proulx, R., Rheault, G., Bonin, L., Torrecilla-Roca, I., Martin, C.A., Desrochers, L., Seiferling, I., 2015. How much biomass do plant communities pack per unit volume? *PeerJ* 3, e849. <https://doi.org/10.7717/peerj.849>.
- Redding, T., Devito, K., 2011. Aspect and soil textural controls on snowmelt runoff on forested Boreal Plain hillslopes. *Hydrol. Res.* 42, 250–267. <https://doi.org/10.2166/nh.2011.162>.
- Ren, J., Vanapalli, S.K., 2019. Comparison of Soil-Freezing and Soil-Water Characteristic Curves of Two Canadian Soils. *Vadose Zone J.* 18 (1-14), 180185. <https://doi.org/10.2136/vzj2018.10.0185>.
- Richardson, J.B., 2017. In: Bobrowsky, P., Marker, B. (Eds.), *Critical Zone, Encyclopedia of Engineering Geology.* Springer International Publishing, Cham, pp. 1–5.
- Rivard, C., Vigneault, H., Piggott, R.A., Larocque, M., Antil, F., 2009. Groundwater recharge trends in Canada. *Can. J. Earth Sci.* 46.

- Rivard, C., Paniconi, C., Bordeleau, G., Lavoie, G., Crow, H., Menses-Vega, B.J., Kononovs, D., Alessia, D.S., Degenhardt, D., Xu, B., Konstantinovskaya, E., Haeri Ardakani, O., Lavoie, R., Aubin, I., McClain, C., 2023. The Fox Creek project: A multi-disciplinary joint endeavour to assess the cumulative effects of 50 years of intensive oil and gas activities. In: Session H54. San Francisco.
- Scanlon, B.R., Christman, M., Reedy, R.C., Porro, I., Simunek, J., Flerchinger, G.N., 2002. Intercode Comparisons for Simulating Water Balance of Surficial Sediments in Semiarid Regions. *Water Resour. Res.* 38, 1323–1339.
- Schneider, R.R., Stelfox, J.B., Boutin, S., Wasel, S., 2003. Manag. Cumul. Impacts Land Uses West. Can. Sediment. Basin.: A Model. Approach. <https://doi.org/10.5751/ES-00486-070108>.
- Schneider, R.R., Devito, K., Kettridge, N., Bayne, E., 2016. Moving beyond bioclimatic envelope models: integrating upland forest and peatland processes to predict ecosystem transitions under climate change in the western Canadian boreal plain. *Ecohydrology* 9, 899–908. <https://doi.org/10.1002/eco.1707>.
- SigMAP, 2023. SigMAP. <https://sigmap.sigmaex.com/public/>.
- Smerdon, B.D., Klassen, J., Gardner, W.P., 2019. Hydrogeological characterization of the Upper Cretaceous–Quaternary units in the Fox Creek area, west-central Alberta. *Alberta Energy Regulator / Alberta Geological Survey, AER/AGS Report 98*, 35–p.
- Smerdon, B.D., Mendoza, C.A., Devito, K.J., 2008. Influence of subhumid climate and water table depth on groundwater recharge in shallow outwash aquifers. *Water Resour. Res.* 44, 2007WR005950. <https://doi.org/10.1029/2007WR005950>.
- Strong, W.L., G.H. La. Roi, 1983a. Root-system morphology of common boreal forest trees in Alberta, Canada. *Can. J. For. Res.* 13 (6), 1164–1173.
- Strong, W.L., G.H. La. Roi, 1983b. Rooting depths and successional development of selected boreal forest communities. *Can. J. For. Res.* 13.
- Tam, B.Y., Szeto, K., Bonsal, B., Flato, G., Cannon, A.J., Rong, R., 2019. CMIP5 drought projections in Canada based on the Standardized Precipitation Evapotranspiration Index. *Can. Water Resour. J. / Rev. Can. Des. Ressour. Hydr.* 44, 90–107. <https://doi.org/10.1080/07011784.2018.1537812>.
- Thompson, C., Mendoza, C.A., Devito, K.J., 2017. Potential influence of climate change on ecosystems within the Boreal Plains of Alberta. *Hydrol. Process.* 31, 2110–2124. <https://doi.org/10.1002/hyp.11183>.
- Van Dongen, A., Jones, C., Schoonmaker, A., Harvey, J., Degenhardt, D., 2023. The influence of forest harvesting activities on seismic line tree and shrub regeneration in upland mixedwood boreal forests. *Can. J. Res. cjfr-2022-0184*. <https://doi.org/10.1139/cjfr-2022-0184>.
- Van Rensen, C.K., Nielsen, S.E., White, B., Vinge, T., Lieffers, V.J., 2015. Natural regeneration of forest vegetation on legacy seismic lines in boreal habitats in Alberta's oil sands region. *Biol. Conserv.* 184, 127–135. <https://doi.org/10.1016/j.biocon.2015.01.020>.
- Waddington, J.M., Morris, P.J., Kettridge, N., Granath, G., Thompson, D.K., Moore, P.A., 2015. Hydrological feedbacks in northern peatlands. *Ecohydrology* 8, 113–127. <https://doi.org/10.1002/eco.1493>.
- Waksman, S., Selman, A., Stevens, K.R., 1930. A Critical Study of the Methods for Determining the Nature and Abundance of Soil Organic Matter. *Soil Sci.* 30.
- Wang, T., Hamann, A., Spittlehouse, D., Carroll, C., 2016. Locally downscaled and spatially customizable climate data for historical and future periods for North America. *PLoS ONE* 11.
- Wang, T., Zhang, H., Zhao, J., Guo, X., Xiong, T., Wu, R., 2021. Shifting Contribution of Climatic Constraints on Evapotranspiration in the Boreal Forest. *Earth'S. Future* 9, e2021EF002104. <https://doi.org/10.1029/2021EF002104>.
- Wang, Y., Hogg, E.H., Price, D.T., Edwards, J., Williamson, T., 2014. Past and projected future changes in moisture conditions in the Canadian boreal forest. *For. Chron.* 90, 678–691. <https://doi.org/10.5558/tfc2014-134>.
- Wei, X., Zhang, M., 2010. Quantifying streamflow change caused by forest disturbance at a large spatial scale: A single watershed study: Large-Scale Forest Disturbance. *Water Resour. Res.* 46. <https://doi.org/10.1029/2010WR009250>.
- Wei, X., Giles-Hansen, K., Spencer, S.A., Ge, X., Onuchin, A., Li, Q., Burenina, T., Ilintsev, A., Hou, Y., 2022. Forest harvesting and hydrology in boreal Forests: Under an increased and cumulative disturbance context. *For. Ecol. Manag.* 522, 120468. <https://doi.org/10.1016/j.foreco.2022.120468>.
- Weiland, L., Green-Harrison, T., Ketcheson, S., 2023. The Influence of Seismic Lines on Wildfire Potential in the Boreal Region of Northern Alberta, Canada. *Forests* 2023 14, 1574. <https://doi.org/10.3990/fl4081574>.
- Worrall, J.J., Rehfeldt, G.E., Hamann, A., 2013. Recent declines of *Populus tremuloides* in North America linked to climate. *For. Ecol. Manag.* 299, 35–51. <https://doi.org/10.1016/j.foreco.2012.12.033>.
- Yin, Z., Ouyang, H., Xu, X., Zhou, C., Zhang, F., Shao, B., 2010a. Estimation of Evapotranspiration from Faber Fir Forest Ecosystem in the Eastern Tibetan Plateau of China Using SHAW Model. *JWARP* 02, 143–153. <https://doi.org/10.4236/jwarp.2010.22017>.
- Yin, Z.F., Ouyang, H., Chen, H., 2010b. Simulating soil freezing and thawing of temperate desert ecosystem on the Qinghai-Tibet Plateau. *Procedia Environ. Sci.* 2, 476–485. <https://doi.org/10.1016/j.proenv.2010.10.052>.